Comparison of GST (Ge-Sb-Te alloys) growth via MOVPE and MBE

von

Shiyu Hu

Masterarbeit in Materialwissenschaft

vorgelegt der

Fakultät für Georessourcen und Materialtechnik

der RWTH Aachen

eingereicht im

November 2020

angefertigt am

Peter Grünberg Institut (PGI-9)

Forschungszentrum Jülich

Bei

Prof. Dr. Lars Peters

Zweitgutachter: Prof. Dr. Detlev Grützmacher

Abstract

Nowadays, the amount of data created every day is much higher than ever before. Conventional silicon based computing technology has reached to its upper physical limits of design complexity, memory, and energy consumption. Therefore, there is need of searching for new material systems, which can overcome all these conventional limitations.

In the memory based materials, one of the categories is phase-change material. It has already been ultilized into random-access memory. In the future, the main aim is to apply the phase-change materials into the low power devices, which can be realized by interfacial phase-change materials.

The family of $Ge_xSb_yTe_z$ (GST) stoichiometric alloys is one of the candidates for bulk phase-change material as well as interfacial phase-change material. In order to utilize them properly, high crystal quality of GST alloys must be achieved.

This thesis has been dedicated to grow GST alloys via Metal-Organic Vapor Phase Epitaxy (MOVPE) and Molecular Beam Epitaxy (MBE). And the nanostructures of GST alloys have been realized via MBE. The structural quality has been investigated by x-ray diffraction (XRD), rocking curve (RC), phi-scan, and reciprocal space map (RSM), while the surface topography has been studied by scanning electron microscopy (SEM) and atomic force microscopy (AFM).

In the future, the stoichiometric states can also be applied to selective area epitaxy via MOVPE, and then incorporated into the fabrication industry.

Contents

List of Abbreviations

CD	Compact disks
DVD	Digital versatile disks
GST	Ge-Sb-Te
PCM	Phase change memory
RAM	Random-access memory
PRAM	Phase-change random-access memory
IPCM	Interfacial phase change memory
MOVPE	Metalorganic Vapour-Phase Epitaxy
MOCVD	Metalorganic Chemical Vapour Deposition
MBE	Molecular Beam Epitaxy
RHEED	Reflection high-energy electron diffraction
XRD	X-ray diffraction
vdW	Van-der-Waals
SL	Septuple layer
QL	Quintuple layer
RC	Rocking curve
FWHM	Full width at half maximum
RSM	Reciprocal space map
XRR	X-ray reflectivity
SEM	Scanning electron microscopy
SE	Secondary electrons
BSE	Backscattered electrons
AFM	Atomic force microscopy
SPM	Scanning probe microscopy
HNF	Helmholtz Nano Facility
PGI	Peter Grünberg Institute
TESb	Triethylantimony
DETe	Diethyltelluride

IPA	Isopropyl alcohol
DI water	Deionized water
TGF	Total gas flow
RMS	Root-Mean-Square
SAE	Selective area epitaxy

1 Introduction

In the process of human development, important information is stored to use it again. The ability to store information has a huge influence on human development. From ancient cave paintings to modern computers, storage technology has been rapidly developed [3]. However, we are facing a challenge of finding the noval storage media to enhance the storage ability.

In the last few decades, optical disks (CDs and DVDs) have been successfully applied for data storage. In order to increase the capacity and density of data storage, new storage media must be found and applied. Phase-change materials (PCMs) can be regarded as a promising candidate, which transform their physical characteristics by absorbing or releasing energy. Among different classes of PCMs, solid-solid transformable materials are the most interesting group for micro/nano-electronics. Only solid-state materials have the capability of incorporation into CMOS-based fabrication industry. Solid-state PCMs can transform from crystalline state to either amorphous state or into another crystalline state. Therefore, they can be used for switching, like oxide-based memristors (depicted in Figure 1.1) or layer-based material switches. Such materials can be used for memory cells in better systems of advanced neurotec processing. [3, 4]

The group of GST (Ge-Sb-Te) stoichiometric alloys is a conspicuous member of conventional PCMs. They can be switched reversible between a crystalline state and an amorphous state, which have different electrical resistivities. The crystalline state of GST alloys has a lower resistance, while the amorphous state has a higher resistance. In GST alloys, the crystalline and amorphous states with different electrical resistivities can be utilized as the logic states for the data storage and non-volatile random-access memory (RAM). [3-6]

GST alloys can also be modeled in form of $GeTe/Sb_2Te_3$ heterostructures. In this form, the material transforms from homogeneous layer stacks to pseudo-binary heterostructures or alters the atomic arrangements in the pseudo-binary heterostructures forming hybrid layer stacks. Compared to conventional PCM, it has primary advantages. The transition of iPCM between SET and RESET states is quicker than that in conventional PCM. Besides, it saves more power than conventional PCM. [19-23]

This thesis focuses on the epitaxy and characterization of conventional GST stoichiometric alloys. GST alloys are grown via Metal-Organic Vapor Phase Epitaxy (MOVPE) discussed in chapter 4 and Molecular Beam Epitaxy (MBE) discussed in chapter 5. The surface topographies of GST samples are measured

by scanning electron microscopy (SEM) and atomic force microscopy (AFM). The compositions are tested by X-ray diffraction (XRD). In addition, the quality of the samples is measured by rocking curve (RC), phi-scan, and reciprocal space map (RSM).

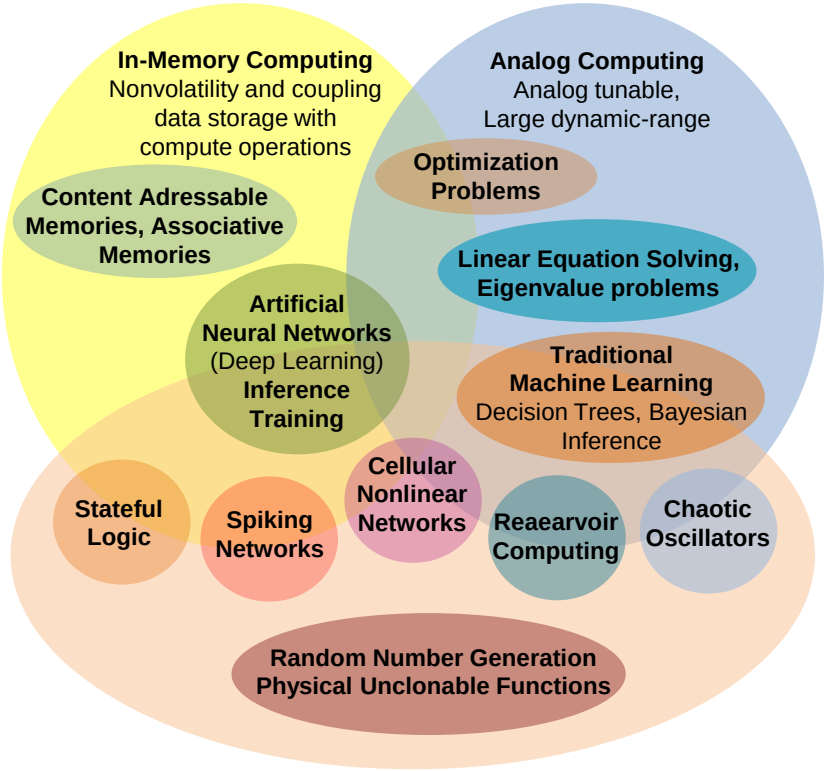

Figure 1.1: Computing application supported by memristive devices, adopted from [55].

2 Theoretical Background of PCMs

In this chapter, phase-change materials (PCMs) and GST alloys are introduced. In section 2.1, PCM and its operational principle are introduced. In section 2.2, GST alloys are introduced. In section 2.3, interfacial phase-change memory (iPCM) is discussed as an attractive candidate for the next generation of non-volatile data storage [1].

2.1 Phase-change materials (PCMs)

Phase-change material (PCM) can transform its physical characteristics by absorbing or releasing energy. Among them, solid-solid transformable materials are the most interesting candidate for micro/nano-electronics. Only solid-state materials can incorporate into CMOS-based fabrication industry. Solid-state PCMs can transform from crystalline state to either amorphous state or into another crystalline state, which could be referred to SET and RESET in the logic states. [3, 4]

In Figure 2.1, one conventional PCM cell is represented as well as its principle. In order to reset the PCM cell into an amorphous state, a large electrical current impulse is applied for a short period. After that, the programming region is melted and then quickly quenched. To switch the PCM cell back into a crystalline state, a medium electrical current is applied for a long time. Therefore, the programming region anneals between the crystallization temperature and the melting temperature. [10, 11]

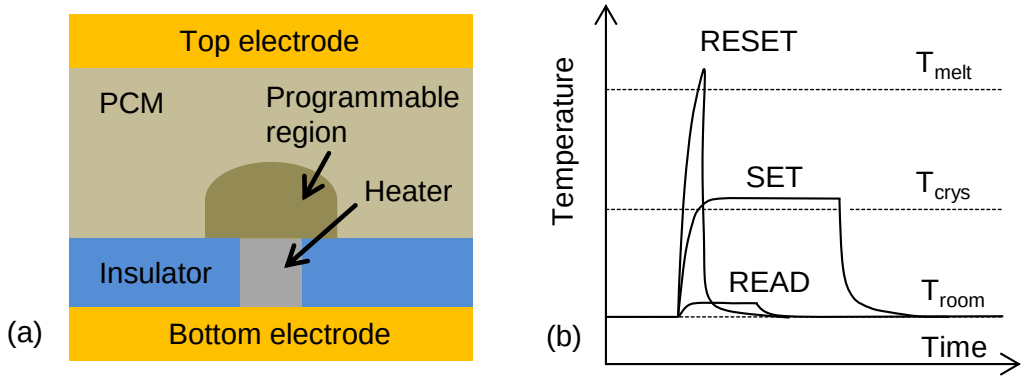

Figure 2.1: The conventional PCM memory cell and its operational principle, adopted from [11]. Left: The cross-section schematic of a conventional PCM cell. Right: PCM cells are programmed and read by applying electrical or optical impulses.

The current-voltage characteristic of the SET and RESET states of PCM cell is depicted in Figure 2.2. Below the threshold switching voltage, the resistance of SET differs from the resistance of RESET. The amorphous state has a higher resistance, which limits the current of the PCM cell. As a result, the PCM cell can not be crystallized by the Joule heating. [10-12]

At the threshold voltage, the high-resistive state starts transferring to a low-resistive state. If a higher voltage than the threshold voltage is applied longer than crystallization time, it leads to memory switching and the cell reaches the low-resistance. Typically, the SET programming time could be achieved in the range of 100-200ns. The energy is mainly consumed by the RESET programming. [12]

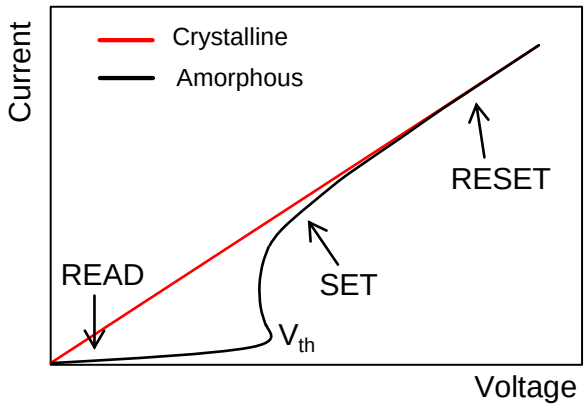

Figure 2.2: Current-voltage characteristic of SET and RESET states of a PCM cell, adopted from [11]. The crystalline state is shown with a red line. The amorphous state is depicted with a black line.

2.2 GST Alloys

The family of GST stoichiometric alloys is an important member of solid-solid transformable PCMs. They have many unique properties [3, 6]:

- Reversible switching between a crystalline state and an amorphous state.
- Switching speed is quick (in nanoseconds level).
- Long-term thermal stability. As a result, they can be utilized as non-volatile memory to store information for a long period.
- Rewritable.

GST alloys can be represented with a ternary phase diagram [5] shown in Figure 2.3. As seen, three classes of phase-change materials are distinguished:

- The pseudo-binary GeTe-Sb_2Te_3 group (shown with the red line): The bigest family of GST alloys. Various combinations of GeTe and Sb_2Te_3 provide different stoichiometric states, such as Sb_2Te_3, $GeSb_4Te_7$, $GeSb_2Te_4$, and $Ge_2Sb_2Te_5$.
- Doped Sb_2Te group.
- Doped Sb group, for example Ge_xSb_{1-x}.

Among the mentioned alloys, $GeSb_4Te_7$ and $GeSb_2Te_4$ are of main interest in this thesis. In order to simplify the representation of the stoichiometric GST alloys, $GeSb_4Te_7$, $GeSb_2Te_4$, and $Ge_2Sb_2Te_5$ will be expressed in forms of GST-147, GST-124, and GST-225 in this thesis.

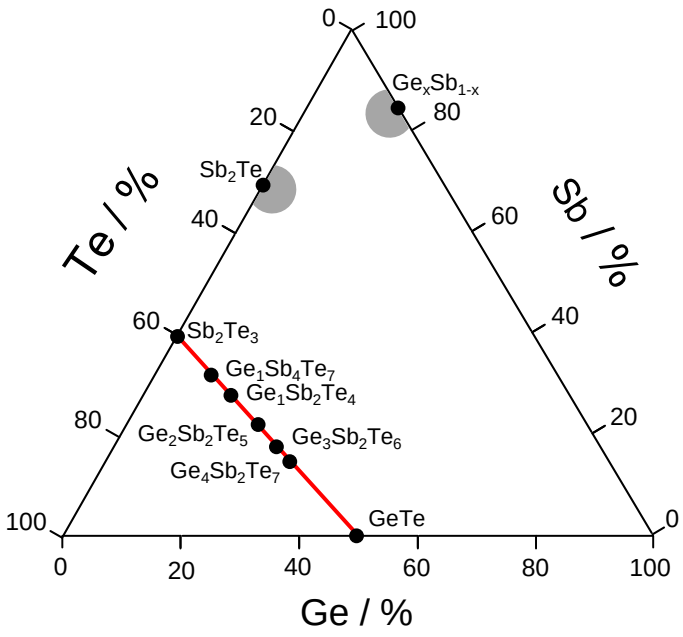

Figure 2.3: Ternary phase diagram of GST alloys, adopted from [5]. This diagram can be divided into three parts: the pseudo-binary GeTe-Sb_2Te_3 group (red line), doped Sb_2Te group, and doped Sb group, for example Ge_xSb_{1-x}.

The unit cells and atomic arrangments of Sb_2Te_3, GST-147, GST-124, and GST-225 are depicted in Figure 2.4. GST alloys have trigonal crystal structure. During switching, they crystallize in a metastable rock-salt structure. In this structure, the anion lattice sites are occupied by Te atoms, while the cation lattice sites are occupied by Ge and Sb atoms as well as vacancies. GST alloys have on average more than four valence electrons per atoms so that bonding by the p-electrons is more favorable. Therefore, the atoms in GST alloys prefer to form an octahedral-like atomic arrangement. [2, 7]

The superlattice of GST crystals is the combination of base layers connected by van-der-Waals (vdW) interactions interactions (shown by the imaginary lines). Sb_2Te_3 is the superlattice of quintuple layers (QL), while GST-124 is made of septuple layers (SL). GST-147 is combination of one Sb_2Te_3 layer and one GST-124 layer. One layer of GST-225 has 9 atoms. Because of the trigonal structure of GST alloys, the number of layers in every unit cell must be multiple of 3.

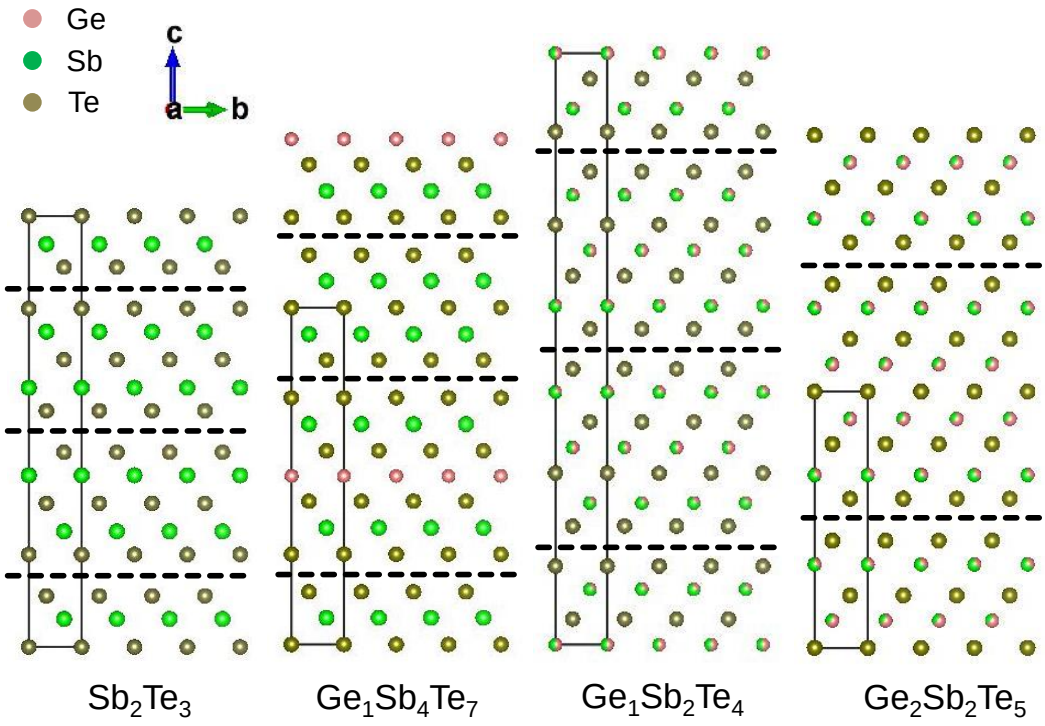

Figure 2.4: Unit cells and atomic arrangments of Sb_2Te_3, GST-147, GST-124, and GST-225. Sb_2Te_3 is a supercell consisting of quintuple layers. GST-124 is a supercell consisting of septuple layers. GST-147 is the combination of one layer GST-124 and one layer Sb_2Te_3. One layer of GST-225 has 9 atoms. Imaginary lines point the placement of vdW gaps.

The stoichiometric GST alloys can also be expressed in form of $(GeTe)_m(Sb_2Te_3)_n$ depicted in Tab. 2.1. In the formula, m and n indicate the total number of GeTe blocks and Sb_2Te_3 QLs in a unit cell. The theoretical lattice constants of GST states can be calculated by the following equation:

$$c_{predicted} = \frac{1}{3}(mc' + nc'') \tag{2.1}$$

In this equation, c' and c'' indicate the out-of-plane lattice constants of GeTe and Sb_2Te_3 c' = 10.66 Å and c'' = 30.45 Å respectively. The theoretical lattice constants of different GST alloys are depicted in Tab. 2.1. [2, 9]

Tab. 2.1: Theoretical lattice constants of GST-147, GST-124, and GST-225.

Material	$(GeTe)_m(Sb_2Te_3)_n$	m:n	a / Å	c / Å
Sb_2Te_3	$(GeTe)_0(Sb_2Te_3)_3$	0:3	4.26	30.45
$GeSb_4Te_7$	$(GeTe)_1(Sb_2Te_3)_2$	1:2	4.25	23.86
$GeSb_2Te_4$	$(GeTe)_3(Sb_2Te_3)_3$	3:3	4.24	41.12
$Ge_2Sb_2Te_5$	$(GeTe)_2(Sb_2Te_3)_1$	2:1	4.22	17.23
GeTe	$(GeTe)_3(Sb_2Te_3)_0$	3:0	4.17	10.66

2.3 Interfacial phase-change materials (iPCMs)

In interfacial phase-change materials (iPCMs), GST alloys have different atomic arrangments from conventional PCMs. They consist of $GeTe/Sb_2Te_3$ heterostructures. [13]

GST-225 can be distinguished from four models (Ferro, Petrov, Inverted Petrov, and Kooi), depicted in Figure 2.5. The first three models are iPCMs, which could be modeled as $(GeTe)_2(Sb_2Te_3)_1$ heterostructures [22]. Two GeTe layers alternate with one Sb_2Te_3 stack. The atomic arrangment of Ge and Te atoms in GeTe layer differ in the three iPCM models. As depicted in Figure 2.5, the atomic arrangment of GeTe in the Ferro model is Ge-Te-Ge-Te, while it is Ge-Te-Te-Ge in the Petrov model. In contrast, the atomic arrangment of GeTe in the inverted Petrov model is Te-Ge-Ge-Te. The last model corresponds to the conventional PCM. [21, 22]

In iPCM, the material transforms from homogeneous layer stacks to pseudo-binary heterostructures or alters the atomic arrangements in the pseudo-binary heterostructures forming hybrid layer stacks [13]. The driving force that leads to switching is still under debate. It is mainly argued between charge injection [14], electric field [15], thermal activation [16], and a combination of Joule heating and electric field [17].

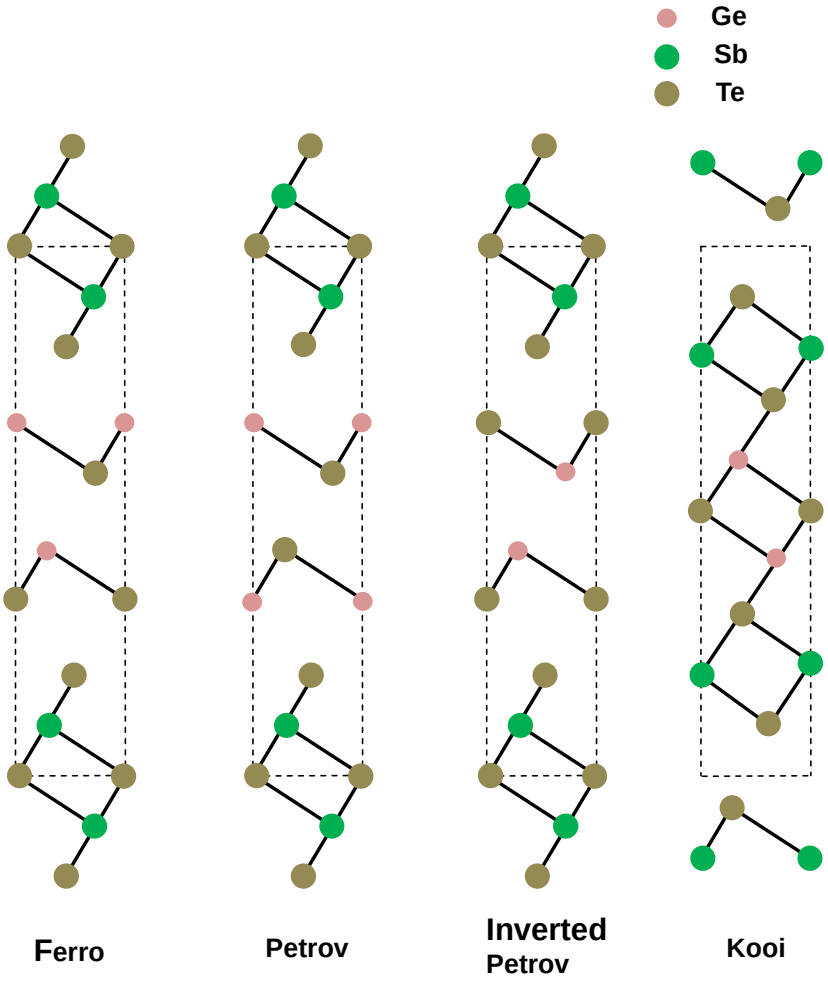

Figure 2.5: Four models of GST-225. The names of the four models from left to right: Ferro, Petrov, Inverted Petrov, and Kooi. The first 3 models are iPCM, and the last model is conventional PCM.

2.3.1 Transformation from conventional PCM to iPCM

Conventional PCMs can be transformed into iPCMs. As introduced, GST-124 is the combination of septuple layers. The left atomic arrangement in Figure 2.6 has two GST-124 layers. As depicted, Ge atoms in the first GST-124 layer can go down to the second GST-124 layer. It forms one GST-225 layer and one Sb_2Te_3 layer. GST-225 can be transformed into $GeTe/Sb_2Te_3$ heterostructures. As a result, conventional GST-124 can be modeled in form of $(GeTe)_3(Sb_2Te_3)_3$ heterostructures. [19-23]

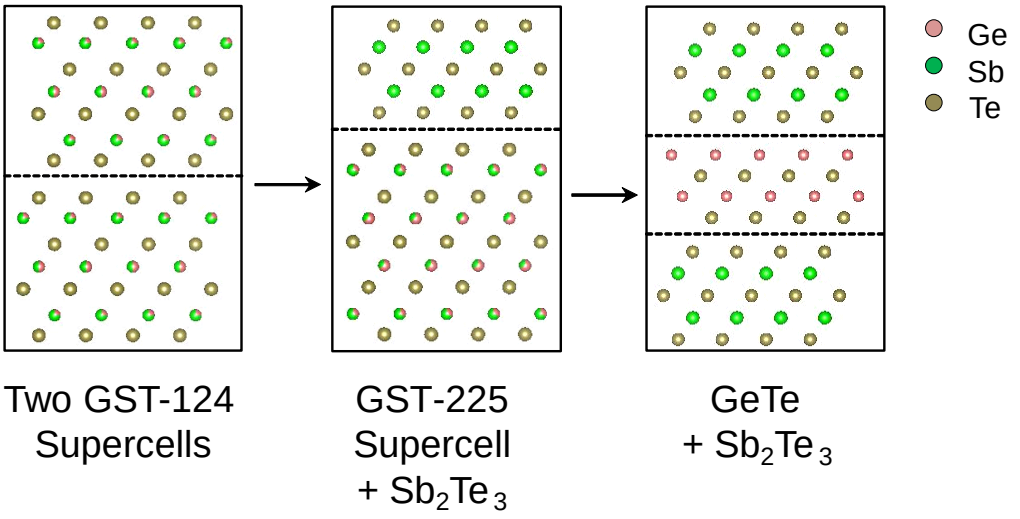

Figure 2.6: Transformation of GST-124 from conventional PCM to iPCM. Left: Two GST-124 layers of conventional PCM. Middle: Model of GST-124 in form of Sb_2Te_3 and GST-225. Right: Model of GST-124 in form of GeTe/Sb_2Te_3 heterostructures.

2.3.2 Advantages of iPCM

Compared to conventional PCMs, iPCMs have conspicuous advantages [19-23]:

- The transition of iPCM between SET and RESET states is quicker. PCMs transform into SET state in 100-200ns, while the transition of iPCMs to SET state is possible in 25ns.
- Interfacial phase-change materials consum less power.

In order to further understand iPCM and the transformation from PCM to iPCM, it is necessary to grow conventional PCMs. In this thesis, conventional GST-124 and GST-147 are the main GST states to deposit.

3 Experimental Methods

In this chapter, attention is paid on experimental methods for GST alloys. In section 3.1, MOVPE is introduced to deposit GST alloys. In section 3.2, MBE is utilized to grow GST alloys. In section 3.3, X-ray is used to test the composition of thin films. In section 3.4, scanning electron microscope is described to measure the surface topographies of the samples. Finally, AFM is used to measure the roughness of GST thin films.

3.1 Metal-Organic Vapour Phase Epitaxy (MOVPE)

Metalorganic Vapour-Phase Epitaxy (MOVPE) is a chemical vapour deposition method producing single- or polycrystalline thin films. [26]

The MOVPE process is schematically illustrated in Figure 3.1. Firstly, the precursors are injected into the reactor of the MOVPE system. Afterward, the precursors undergo pyrolysis in the reactor and the subspecies absorb onto the silicon wafer. Consequently, the precursor subspecies incorporate into an epitaxial layer. [24-28]

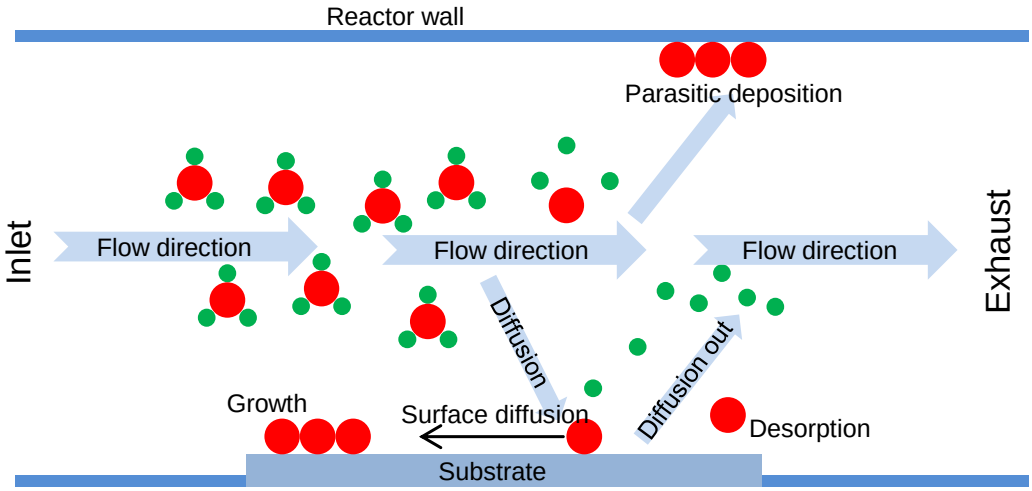

Figure 3.1: Schematic illustration of processes in the MOVPE reactor.

3.1.1 Precursors utilized for epitaxy of GST alloys

In this thesis, digermane [Ge_2H_6], triethylantimony [$(C_2H_5)_3Sb$], and diethyltelluride [$(C_2H_5)_2Te$] are used as precursors to grow GST alloys. The structures of the precursors are shown in Figure 3.2.

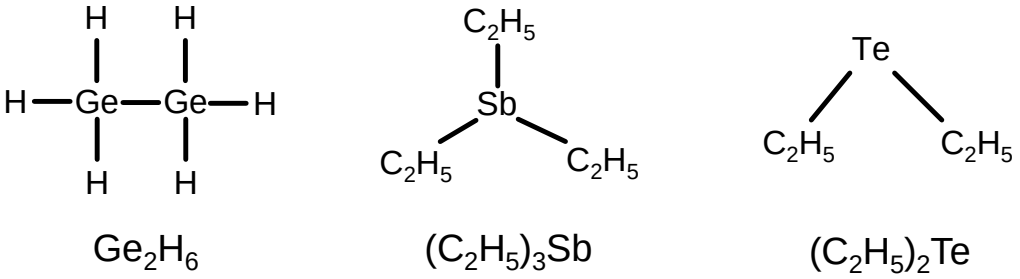

Ge_2H_6 $(C_2H_5)_3Sb$ $(C_2H_5)_2Te$

Figure 3.2: Structures of precursors used in this work. Left: digermane (Ge_2H_6), Middle: triethylantimony (TESb), Right: diethyltelluride (DETe).

The presursors are carried into the reactor by carrier gas N_2. In the reactor, the precursors mix, decompose, and react. The main reactions can be represented as follows [31]:

$$Ge_2H_6 \rightarrow 2\ GeH_3 \tag{3.1}$$

$$GeH_3 + (C_2H_5)_3Sb \rightarrow GeSb + C_2H_6 \tag{3.2}$$

$$2\ GeH_3 + (C_2H_5)_2Te \rightarrow GeTe + 4\ C_2H_4 \tag{3.3}$$

3.1.2 Spin-coating and chemical cleaning of the substrates

The epitaxial growth of GST alloys is performed on a silicon wafer in the orientation of Si(111). GST alloys have trigonal structure. The unit cell of Si substrate is depicted in Figure 3.3. Because of the threefold symmetry in the orientation of Si(111), GST alloys can be deposited with a perfect hexagonal structure on Si(111) [24, 25]. The quality of Si wafers could affect the deposition of GST samples. The main flaw of Si wafers is miscut. The effect of substrate miscut on GST epitaxy will be discussed in section 4.6.2.

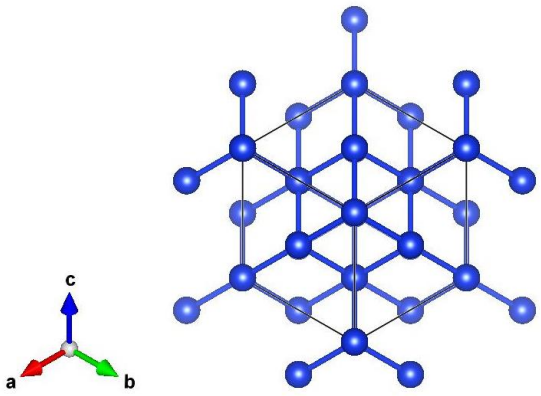

Figure 3.3: The crystal structure of Si(111).

In this work, GST alloys are deposited on a quarter of 2-inch Si(111) wafers. It's shown in Figure 3.4. Before epitaxy of GST alloys, the 2-inch Si wafers must be sawed into four quarters to match the substrates holder in the reactor of MOVPE system. In order to prevent the silicon wafers from contamination by particles, they must be firstly spin-coated in HNF to make an organic film on the substrates. In this thesis, the substrates are spin-coated with the resist (organic: AZ5214E).

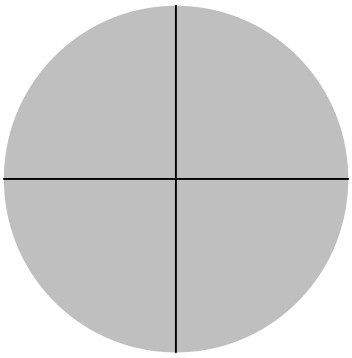

Figure 3.4: A quarter of a 2-inch Si(111) wafer is used as substrate to deposit GST alloys.

Before epitaxy, the silicon wafers must be chemically cleaned to remove the organic films. The procedure of chemical cleaning is depicted in Tab. 3.1. Firstly, the wafer is dipped into acetone for 5 minutes and then transferred into isopropyl alcohol (IPA) for 5 minutes to remove the organic contaminants, which were spin-coated on silicon. Secondly, the wafer is dried it and transferred into the piranha solution for 10 minutes, which is a mixture of 96% sulfuric acid and 31% hydrogen peroxide with the ratio of 1:1. This process removes any residual organic contaminants on the surface. Then the wafer is rinsed in deionized (DI) water for 5 minutes. Finally, the wafer is dipped in 1% hydrofluoric acid for 5 minutes to remove the native oxide.

Tab. 3.1: Chemical cleaning procedures of Si substrates.

Steps	Conditions	Contaminations
Step1	Acetone	Organic
Step2	Isopropyl alcohol (IPA)	Organic
Step3	Piranha	Organic
Step4	1% HF	Native oxide

3.1.3 Bake-out of the reactor

Bake-out is a process of thermal cleaning to remove the parasitic deposition in the reactor shown in Figure 3.1. Parasitic deposition could lead to a memory effect, which influences the quality of the sample [24, 25]. The influence will be discussed in section 4.6.1. In order to clean the reactor, it must be treated with H_2. Bake-out can be divided into 4 steps shown in Tab. 3.2. It takes 15min for every step.

Tab. 3.2: Bake-out and its conditions.

Steps	Conditions	Time
Step1	800°C, 500mbar	15min
Step2	600°C, 10mbar	15min
Step3	800°C, 500mbar	15min
Step4	600°C, 10mbar	15min

For the first step, the reactor is heated with the temperature of 800°C under the reactor pressure in 500mbar for 15min. Then the temperature is reduced to the growth temperature of 600°C, and the reactor pressure is reduced to 10mbar. Afterwards, the temperature is increased again to 800°C, and the reactor pressure is increased to 500mbar. The last step repeats the second step. All of the four steps aim at removing parasitic deposition in the reactor.

3.2 Molecular beam epitaxy (MBE)

Molecular Beam Epitaxy (MBE) is an epitaxial method utilized to grow thin films of various elemental compounds. The diagram of MBE system is depicted in Figure 3.5. In order to deposit GST alloys, Knudsen cells are utilized, which are filled separately with Ge, Sb, and Te metals. In Knudsen cells, the crucibles are heated up with integrated coils to evaporate the desired materials. The stoichiometric GST states are realized by tuning the the temperature of effusion cells, as it controls the individual beam flux of elements (Ge, Sb, and Te). The growth rate which in turns dictates the crystal quality of the epilayer is controlled by the substrates temperature.

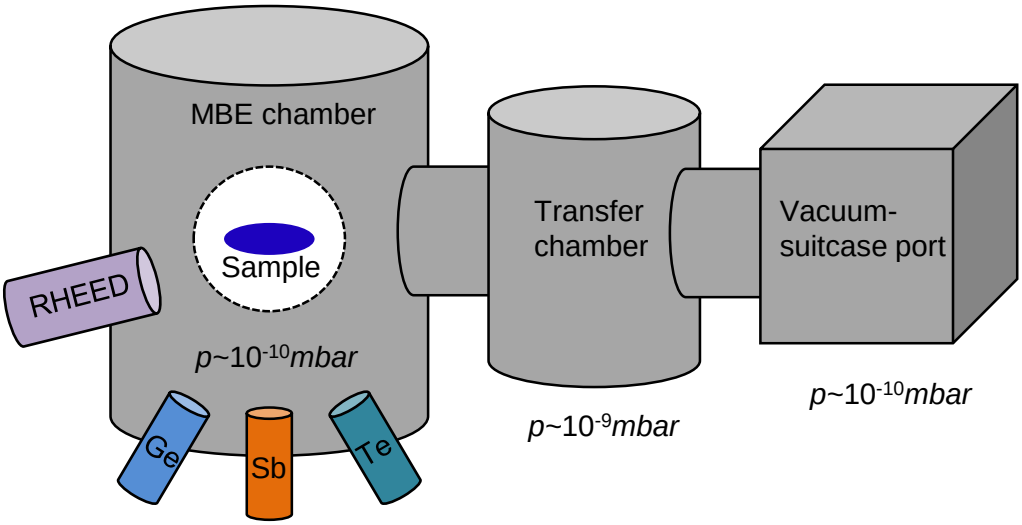

Figure 3.5: Diagram of the MBE system utilized for deposition of stoichiometric GST alloys. In this system, three effusion cells are used to deposit GST samples. The RHEED system is used to investigate the deposition.

The MBE system is divided into three parts: a load lock, a transfer chamber, and the growth chamber depicted in Figure 3.5. The three chambers are separated by shutters. In the growth chamber, the sample is held underneath a grahite substrate heater, which can reach the temperature of 1000°C. The molecular beam sources are mounted to the bottom of the growth chamber facing the surface of the sample. The reflection high-energy electron diffraction (RHEED) system is utilized to observe the formation of GST alloys on silicon.

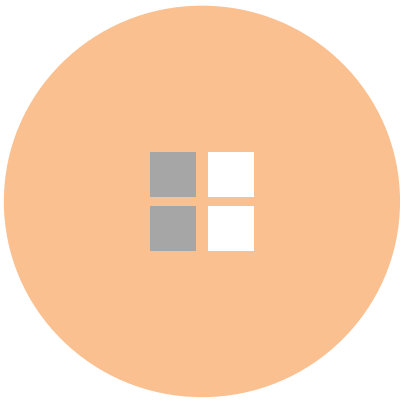

Figure 3.6: The holder utilized for epitaxy of stoichiometric GST alloys on Si(111) in MBE systems.

The stoichiometric GST alloys are deposited on Si(111) with a substrate holder depicted in Figure 3.6. Before deposition, the substrates should also be spin-

coated to prevent from contamination by particles, and then cleaned to remove the contaminations before epitaxy. The procudures are depicted in section 3.1.2. In order to thermally clean the substrates, the wafers should be heated up to 700°C for 25min. Afterwards, the substrates are cooled down to the growth temperature around 285°C.

3.3 X-ray Diffraction (XRD)

X-ray diffraction is a characterization method determining the composition of the epitaxial GST alloys. It is based on constructive interference of monochromatic X-rays with the crystals. A diffracted ray will be produced through the interaction of the incident rays and the sample, when the condition of Bragg's law is satisfied [34]:

$$2d_{hkl} \sin\theta = n \cdot \lambda \tag{3.4}$$

In this equation, d_{hkl} is the interplant spacing between (hkl) crystal planes, θ is the incident angle between incident X-ray and the crystal plane, n is a positive integer, λ is the wavelength of the X-ray. These diffracted X-rays are then detected and counted. In this thesis, the mode of θ-2θ scan is mainly used. By scanning the sample in range of 2θ, all possible diffraction directions of the lattice should be attained. Because the positions of reflexes vary from different GST crystal composition, the phase of GST crystal can be determined by this mode. In addition, X-ray reflectivity (XRR) measurements can be used to determine the thickness of the epitaxial GST thin films. [34-36]

3.4 Scanning Electron Microscopy (SEM)

A scanning electron microscope produces images of GST alloys by scanning the surface with a focused beam of electrons. Through interaction of electrons and atoms, various signals are produced, which contain information about the surface topographies of the samples. In general, secondary electrons and backscattered electrons (shown in Figure 3.7) are the two main signals producing images. [41]

Secondary electrons (SEs) originate from the inelastic interactions between the primary electron beams and the surface or the near-surface regions of the samples. Backscattered electrons (BSEs) are high-energy electrons re-emitted from the sample due to elastic scattering by atoms. Compared to SEs, backscattered electrons originate from a broad region within the interaction volume. Both of them are very useful for inspecting of the surface topography.

The images of backscattered electrons show high sensitivity to differences in atomic number. In addition, the imagings of backscattered electrons can provide more details of the surface information. [41, 42]

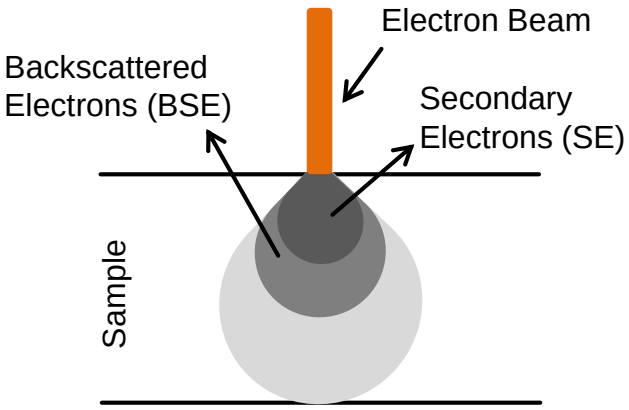

Figure 3.7: Generated secondary electrons (SE) and backscattered electrons (BSE).

3.5 Atomic force microscopy (AFM)

Atomic force microscopy (AFM) is a type of scanning probe microscopy (SPM), which can produce 3-dimensional images of GST alloys with a high resolution. It is realized by scanning the surface of GST alloys with a tip on a spring-like cantilever. The end of the spring-like cantilever is lighted with a laser, which is reflected to a position-sensitive detector. Afterwards, the detector measures the reflected laser and then converts it to electrical signals. [37, 38]

In general, AFM operations can be divided into two modes: contact mode and tapping mode. In this thesis, only tapping mode was used to measure the surface topography of GST samples. In this mode, the cantilever is kept with constant amplitude as long as it has no interaction with the sample. While approaching the sample, the interaction forces change the constant amplitude. As a result, it can be used to control the height of the cantilever over the samples. [37-40]

In this thesis, the maximum resolution of AFM are 512×512 px^2. The scan rate is set between 0.5Hz and 2.0Hz. In addition, the images are taken from an area of 15×15 μm^2. With AFM, the roughness of the GST samples can be evaluated.

4 Epitaxial growth of stoichiometric GST alloys via MOVPE

This chapter focuses on the epitaxial growth and the characterization of GST alloys. In section 4.1, van-der-Waals epitaxy is introduced. In section 4.2, the parameters used for epitaxy of GST alloys are introduced. In section 4.3, the epitaxial growth of Sb_2Te_3 is discussed. In section 4.4, the epitaxial growth of GST-124 is investigated. In section 4.5, GST-147 is grown. In section 4.6, the influence of bake-out and the substrates quality are discussed.

4.1 Van-der-Waals epitaxy

The in-plane lattice constant of GST alloys is around 4.26Å, while the in-plane lattice constant of Si is around 3.88Å. It is about 11% lattice mismatch between GST alloys and the substrate. Therefore, conventional epitaxy is not possible. Before epitaxy, the wafer is pre-treated with Te precursor to grow one layer of Te atoms on Si wafer. The deposited Te layer saturates dangling bonds and helps vdW-epitaxy.

The growth process is divided into four steps:

- Annealing: the wafer is treated at 690°C in H_2 atmosphere for 30min to create the dangling bonds on Si wafers.
- Cooling: the wafer is cooled down to the growth temperature (450°C - 500°C).
- Pretreatment with Te precursor.
- Van-der-Waals Epitaxy.

4.2 Parameters by MOVPE

The epitaxial growth of stoichiometric GST alloys on silicon wafers is influenced by different factors:

- The quality of substrates.
- The growth temperature.
- The total gas flow.
- The pressure of the reactor.
- The partial pressure of the precursors.

In this thesis, the pressure of the reactor is kept constant with 50mbar for all epitaxial growth of GST alloys. The partial pressures of the precursors are also

kept constant with values given in Tab. 4.1 [6]. Only the growth temperature and the gas flow are changed to optimize the quality of the samples. In addition, their influence on the epitaxial growth of GST alloys is researched.

Tab. 4.1: Partial pressures of precursors (Ge_2H_6, TESb and DETe).

Precursors	Partial pressure / mbar
Ge_2H_6	$7.16 \cdot 10^{-3}$
TESb	$4.78 \cdot 10^{-3}$
DETe	$1.33 \cdot 10^{-1}$

Sb_2Te_3 is the base state of GST states. As a result, it is the first material to grow in this thesis. Afterwards, GST-124 is deposited. Because GST-147 is the combination of Sb_2Te_3 and GST-124, it is the last material to deposit.

4.3 Epitaxial growth of Sb_2Te_3

Sb_2Te_3 is only a base state of GST stoichiometric states. The epitaxial growth of Sb_2Te_3 is not the point of this thesis. Therefore, it is not discussed in detail. The epitaxy can be influenced by the total gas flow and the growth temperature. In this section, the total gas flow of 2500sccm and 3000sccm was utilized, and the growth temperature is varied from 450°C to 490°C. The process and parameters used for epitaxy of Sb_2Te_3 are shown in Tab. 4.2.

Tab. 4.2: The process and parameters utilized for epitaxial growth of Sb_2Te_3.

	Annealing	**Cooling**	**Pretreatment**	**Break**	**Growth**
t/min	28+2	11	2	2	40
Carrier gas	H_2	N_2			
Precursors	DETe	--	Ge_2H_6 , TESb	--	DETE , TESb
T/℃	690	decrease	450-490		
P/mbar	50				
TGF/sccm	2600	2200	2600	2200	2500/3000

4.3.1 Characterization of Sb_2Te_3 by SEM and XRD

At the total gas flow of 3000sccm, the samples are better than grown at 2500sccm. The influence of the total gas flow is not discussed in detail in this section. The growth temperature is applied from 450°C to 490°C with 5°C step. At 475°C, the sample is the best one in all of the samples. In order to clearly show the quality of the best sample, the sample grown at 450°C was used as the comparative sample.

The SEM images of the samples grown at 450°C and 475°C are depicted in Figure 4.1. As revealed, at the growth temperature of 450°C, the film is not coalesced on Si wafer. In contrast, a total coalesced film on Si substrate was realized at 475°C.

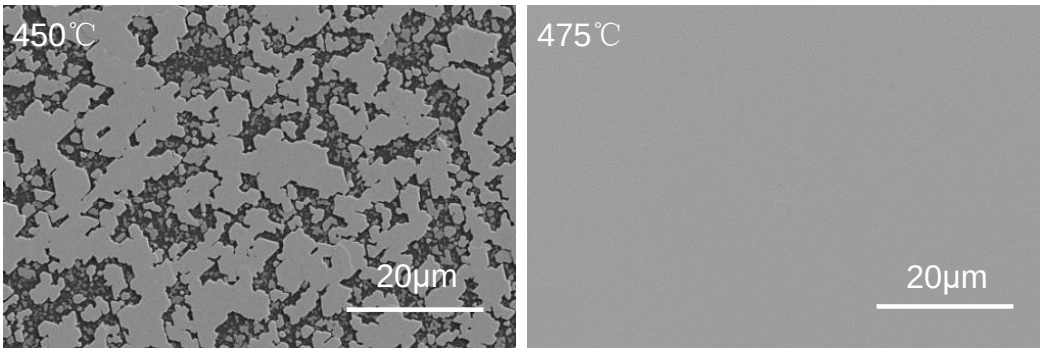

Figure 4.1: SEM images of Sb_2Te_3 grown on Si(111) with different growth temperatures. Left: Epitaxy at 450°C, right: Epitaxy at 475°C.

In order to investigate the composition of the samples, they were measured with XRD. The XRD results are depicted in Figure 4.2. As shown, both of the samples are composed of Sb_2Te_3.

The rocking curve of the samples was measured with the diffraction peak of Sb_2Te_3(0015) at around $2\theta=45°$. A smaller FWHM value confirms that the sample has a better quality. As revealed in Figure 4.2, FWHM value of Sb_2Te_3 sample grown at 450°C is 864, and it is 484 with the applied growth temperature of 475°C. Therefore, the sample grown at 475°C is better than that grown at 450°C.

In order to further investigate the quality of the sample, it was measured by atomic force microscopy (AFM) and reciprocal space map (RSM).

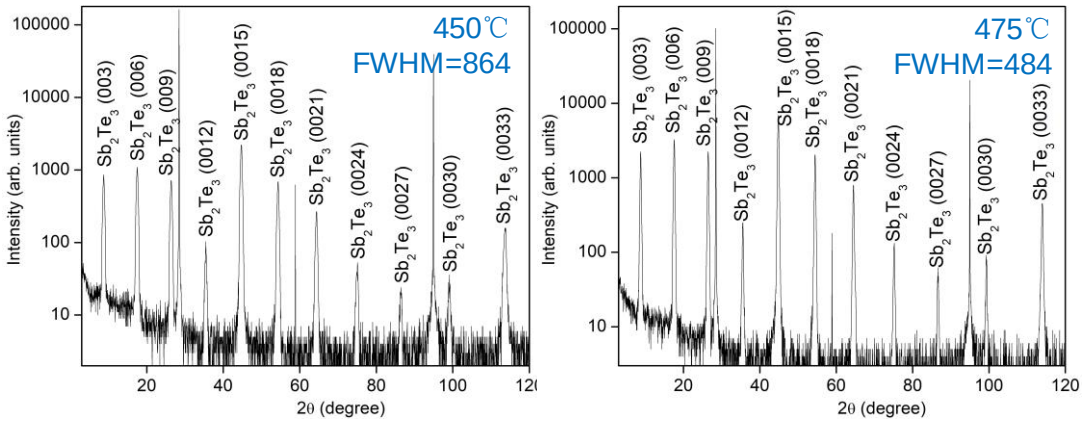

Figure 4.2: XRD images of Sb_2Te_3 grown on Si(111) with different growth temperature. Left: Epitaxy at 450°C, right: Epitaxy at 475°C. Rocking curve was measured with the peak Sb_2Te_3(0015) at around 2θ=45°. (XRD performed by Dr. Alexander Shkurmanov)

4.3.2 Characterization by AFM and RSM

At the growth temperature of 475°C, coalesced Sb_2Te_3 has been grown. In order research its surface topography, it was scanned by AFM with a scan area 15×15 μm^2. The characterization results are depicted in Figure 4.3. The RMS roughness was calculated with value of 2.1nm. The height of Sb_2Te_3 surface fluctuates in a range of 5nm. It reveals that the surface of Sb_2Te_3 is smooth.

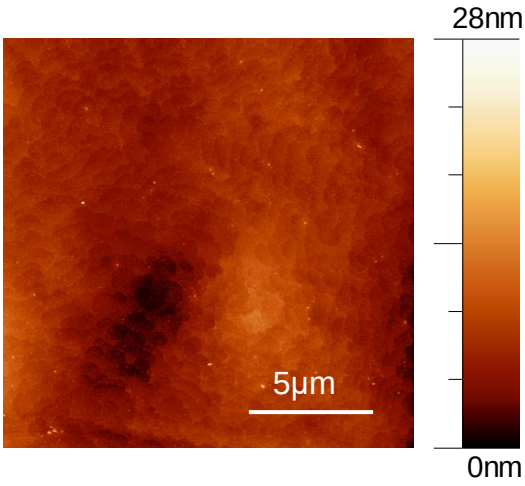

Figure 4.3: AFM characterization of Sb_2Te_3 grown on Si(111) with the applied growth temperature of 475°C. The scan area is 15×15 μm^2.

Afterwards, the lattice parameters were measured by reciprocal space map (RSM) around (1 0 23) reflection of Sb_2Te_3. The result is depicted in Figure 4.4. Intensity profiles were extracted from the map and are depicted on the top and right-hand side of the picture. The lattice constants are found to be equal to a=4.37 ± 0.03Å

and c=30.27 ± 0.06Å. By this method, lattice parameters were measured with a low precision.

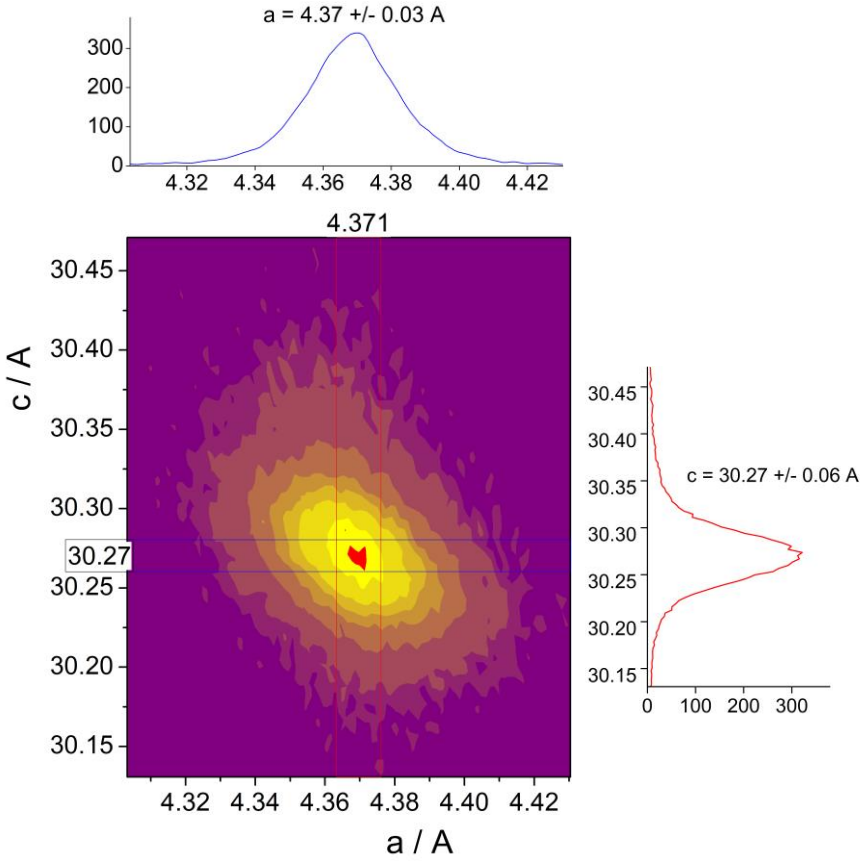

Figure 4.4: Reciprocal space map (RSM) around (1 0 23) reflection of Sb_2Te_3 deposited at 475°C with the total gas flow of 3000sccm. (RSM performed by Dr. Gregor Mussler and Dr. Alexander Shkurmanov)

The out-of-plane lattice parameter can also be calculated by the equation depicted in Figure 4.5:

$$\sin(\theta I) = \frac{\lambda I}{2c} \tag{4.1}$$

In this equation, I is the index of the diffraction peak, λ is the wavelength of x-ray, θI is the degree of the corresponding diffraction peak, and c is the out-of-plane lattice parameter.

According to the information in XRD image, the relationship diagram (depicted in Figure 4.5) between $\sin(\theta I)$ and index can be made. The out-of-plane lattice parameter was calculated with value: c=30.33 ± 0.01Å. This method can improve

the precision of out-of-plane lattice parameter. However, the in-plane lattice parameter can not be determined by this method.

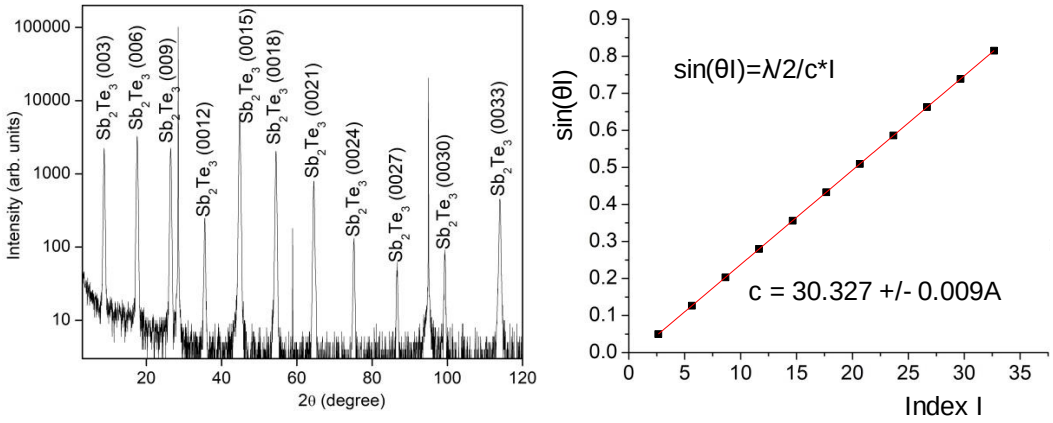

Figure 4.5: Left: XRD image of Sb_2Te_3; Right: The relationship diagram between $\sin(\theta I)$ and index. (XRD performed by Dr. Gregor Mussler and Dr. Alexander Shkurmanov)

According to the methods, the experimental lattice parameters can be measured with the values: a=4.37 ± 0.03Å, c=30.33 ± 0.01Å. They differ slightly from the values reported in the literature: a=4.26Å, c=30.45Å [30]. Compared to the theoretical lattice constants, the in-plane lattice parameter is larger, while the out-of-plane lattice parameter is smaller. The discrepancy from the theoretical value suggests an in-plane tensile strain, which is not expected as vdW crystals grow fully relaxed independent of the substrate.

As revealed by the characterization results, Sb_2Te_3 with high quality was realized at the growth temperature of 475°C with the total gas flow of 3000sccm. These parameters can be ultilized as the base to grow GST alloys by increasing Ge flow.

4.4 Epitaxial growth of stoichiometric state GST-124

This section aims at epitaxial growth of state GST-124 by optimizing of the total gas flow and the growth temperatures. The process and parameters utilized for epitaxy of GST-124 are depicted in Tab. 4.3.

Tab. 4.3: The process and parameters used for epitaxial growth of GST-124.

	Annealing	Cooling	Pretreatment	Break	Growth
t/min	28+2	11	2	2	60
Carrier gas	H_2	N_2			
Precursors	DETe	--	Ge_2H_6 , TESb	--	Ge_2H_6 , DETE , TESb
T/℃	690	decrease	475-495		
P/mbar	50				
TGF/sccm	2600	2200	2600	2200	2500 or 3000

4.4.1 The influence of the growth temperature on GST-124

The growth temperature is investigated as the first variable parameter, which is varied from 475°C to 495°C with 5°C step. The total gas flow is kept constant with 2500sccm. Respective flows of the 3 precursors are depicted in Tab. 4.4.

Tab. 4.4: Respective flows of the 3 precursors at the total gas flow of 2500sccm.

Total gas flow	Ge_2H_6 flow	TESb flow	DETe flow
2500sccm	15sccm	34.7sccm	249.4sccm

After epitaxial growth, the coalescence of the samples is primarily investigated by SEM. The SEM images of GST samples grown on Si(111) from 475°C to 495°C with 5°C step are depicted in Figure 4.6. As shown, GST alloys tend to island growth at 475°C. It formed many trigonal islands on the surface. And the thin film is not coalesced on Si substrate. With an increased growth temperature, trigonal islands disappeared. Si substrate is totally covered by GSTalloys. At 490°C, the sample was found very smooth.

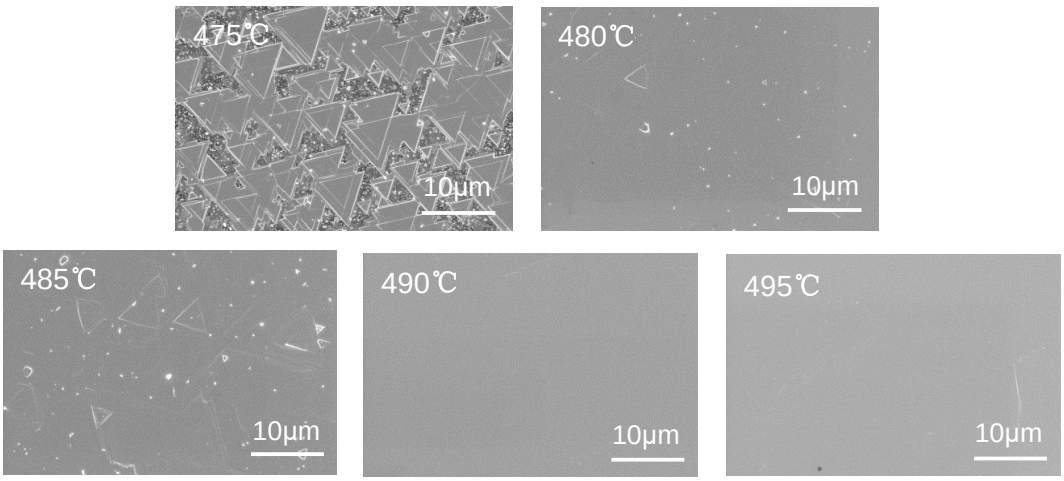

Figure 4.6: SEM images of GST samples grown on Si(111) from 475°C to 495°C with 5°C step at the total gas flow of 2500sccm.

Afterwards, the samples were scanned by XRD to measure their compositions. The XRD images are depicted in Figure 4.7. With the applied growth temperature of 475°C, the GST sample is composed of a mixture phase of GST-225 and GST-124. With an increased growth temperature, the composition of GST samples shifts gradually from the mixture phase to GST-124. Accordingly, the ratio of Ge in GST alloys reduces. The reason will be discussed in the following sentences with Figure 4.8. At 490°C and 495°C, GST samples are composed of GST-124.

The rocking curve was measured with the diffraction peak of GST-124(0021). At 490°C, FWHM value of GST-124 is 577, and at 495°C it was measured with value of 706. It confirms that the quality of GST-124 grown at 490°C in different temperature gradients is best.

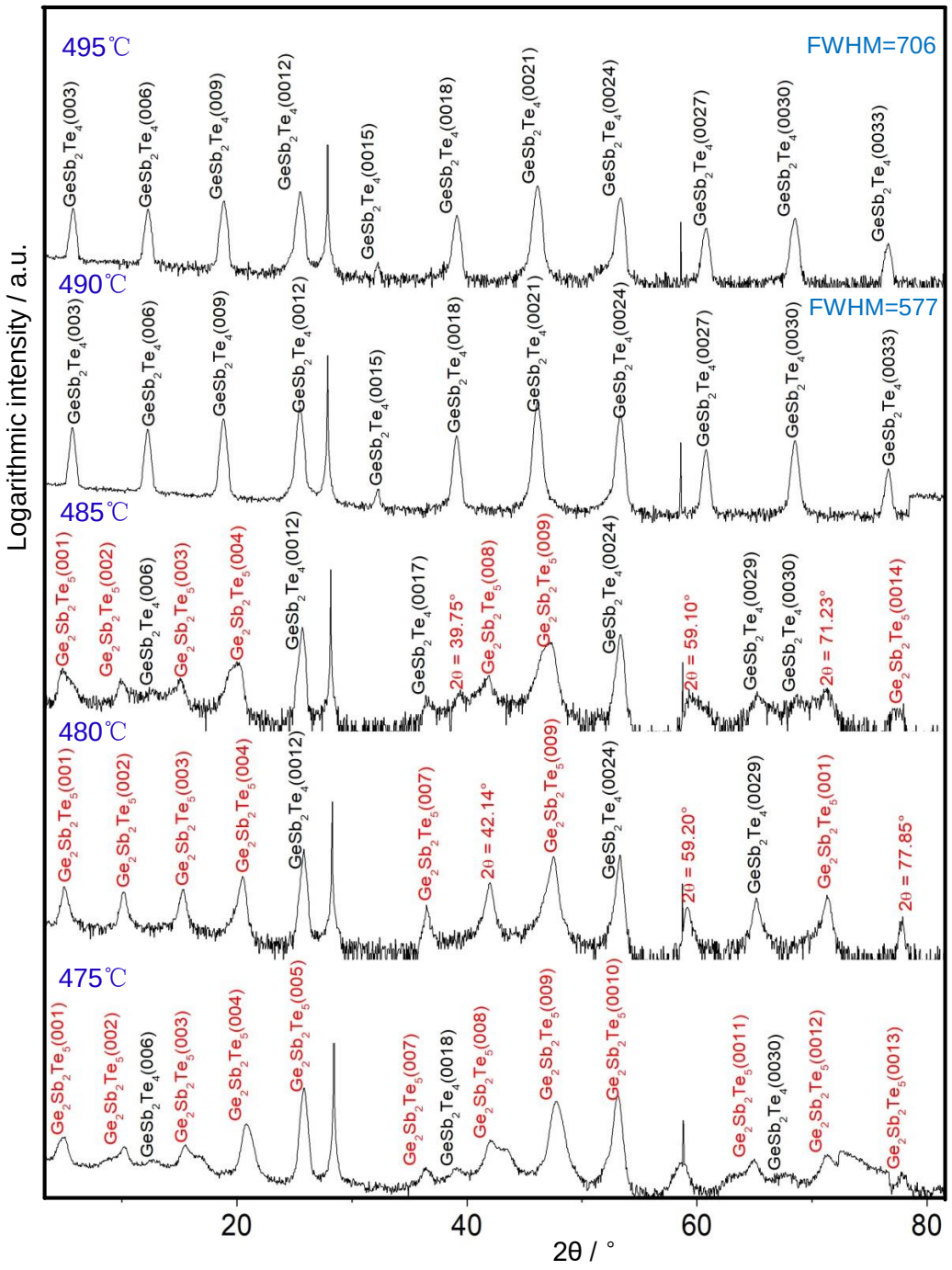

Figure 4.7: XRD images of GST samples grown on Si(111) with the total gas flow of 2500sccm. From bottom to top, the growth temperature increases from 475°C to 495°C. The rocking curve was measured with the peak GST-124(0021) at around 2θ=46°. (XRD performed by Dr. Alexander Shkurmanov)

Explanation: reduction of Ge-ratio in GST alloys with an increased growth temperature

The fraction of decomposed precursors at different temperatures is depicted in Figure 4.8. At 400°C, Ge_2H_6 has been completely decomposed, while TESb and DETe just start to decompose. With an increased temperature, the fraction of decomposed TESb and DETe increases. Equivalently, the ratio of Ge in GST alloys reduces.

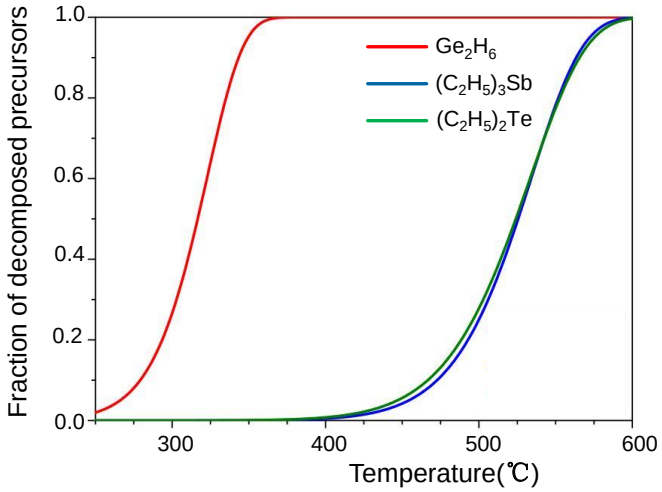

Figure 4.8: Fraction of decomposed precursors at different temperatures, adopted from [25].

4.4.2 The influence of the total gas flow on GST-124

The total gas flow (TGF) is explored as the second variable parameter. This section focuses on the influence of the total gas flow of 2500sccm and 3000sccm on GST-124. When the total gas flow is changed, the respective precursors flow is also changed to keep the partial pressures constant. The change of the total gas flow and the respective precursors flow (depicted in Tab. 4.5) should satisfy:

$$\frac{TGF1}{TGF2} = \frac{X}{X'} \tag{4.1}$$

In this equation, $TGF1$ is the primary total gas flow, and $TGF2$ is the changed total gas flow. X is the primary precursors flow, and X' is the changed precursors flow.

Tab. 4.5: The change of respective precursors flow from the total gas flow of 2500sccm to 3000sccm.

Total gas flow	Ge_2H_6 flow	TESb flow	DETe flow
2500sccm	15sccm	34,7sccm	249.4sccm
3000sccm	18sccm	41.6sccm	299.3sccm

With the applied total gas flow of 3000sccm, the samples were scanned by SEM to measure the coalescence of the thin films. The results are depicted in Figure 4.9. With an increased growth temperature, it shows the same tendency as the samples grown at 2500sccm. At 490°C, the sample was found very smooth.

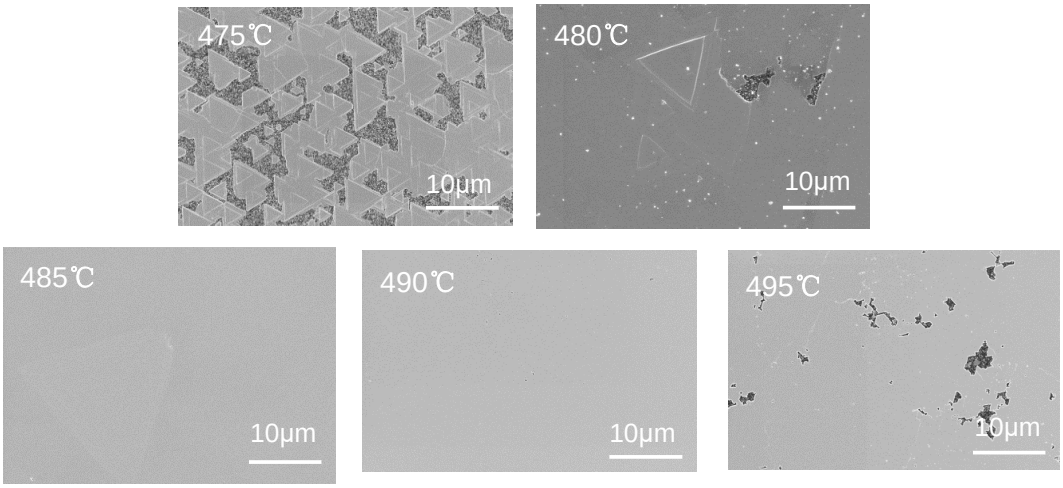

Figure 4.9: SEM images of GST samples grown on Si(111) from 475°C to 495°C with 5°C step at the total gas flow of 3000sccm.

Afterwards, the samples were scanned by XRD to measure their compositions. The XRD images are depicted in Figure 4.10. With the applied growth temperature of 475°C, the GST sample is composed of GST-225. It differs from the sample grown at 2500sccm, which is composed of a mixture phase of GST-225 and GST-124. With an increased growth temperature, it shows the same tendency:

- The composition of GST samples shifts gradually to GST-124.
- The ratio of Ge in GST alloys reduces (The reason has been discussed in last section).

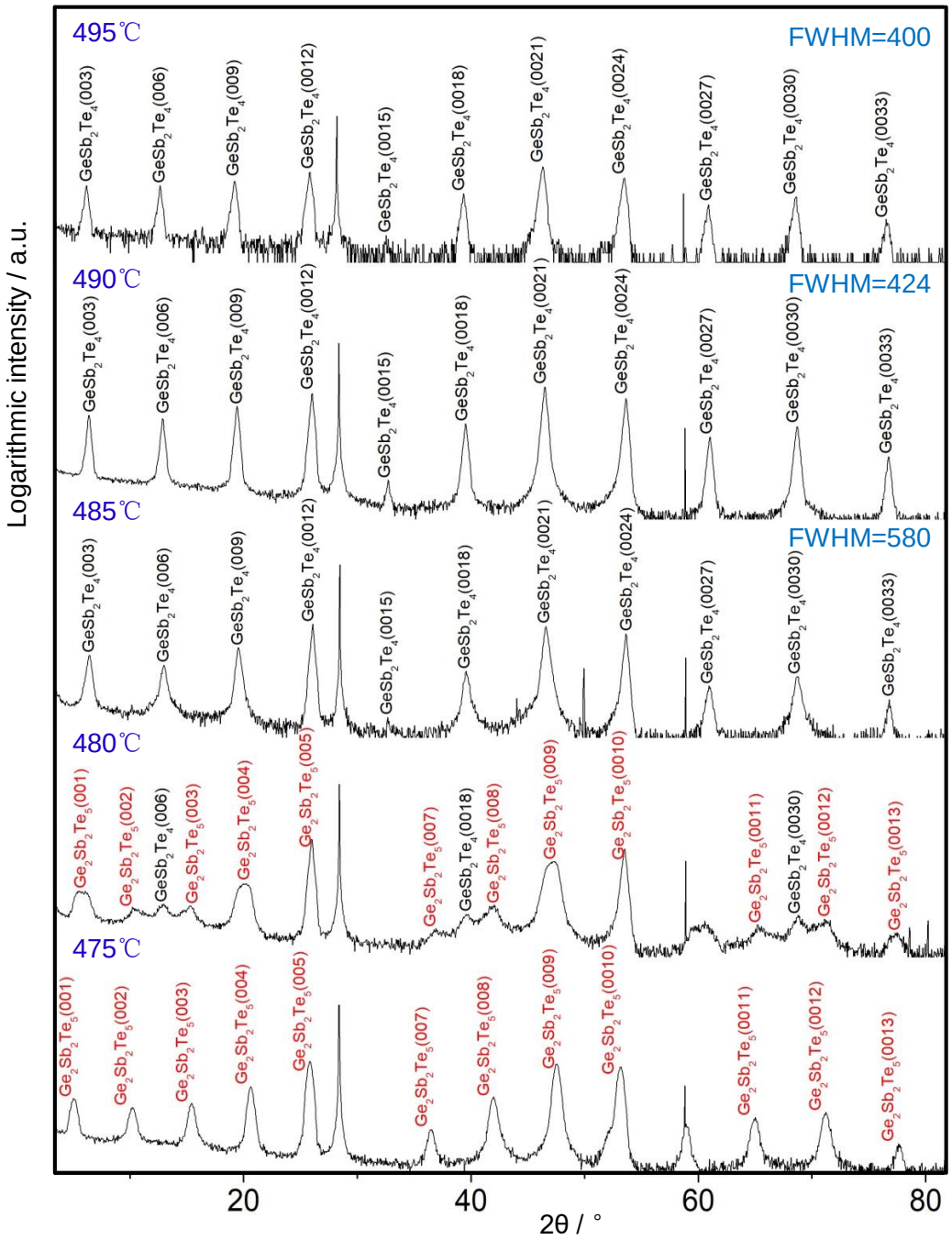

Figure 4.10: XRD images of GST samples grown on Si(111) with the total gas flow of 3000sccm. From bottom to top, the growth temperature increases from 475°C to 495°C. The rocking curve was measured with the peak GST-124(0021) at around 2θ=46°. (XRD performed by Dr. Alexander Shkurmanov)

The rocking curve was measured with the diffraction peak of GST-124(0021). At 490°C, FWHM of GST-124 was measured with value 424 that is lower than that

grown at 2500sccm. Compared to the sample grown at 2500sccm, the quality of the sample grown at 3000sccm is better.

4.4.3 Characterization by AFM and RSM

In the last two sections, it has been discussed that the sample grown at 490°C with the applied total gas flow of 3000sccm is coalesced GST-124. In order to further investigate the samples quality, it is then measured by AFM and RSM.

The AFM image with a scan area 15×15 μm^2 is depicted in Figure 4.11. The RMS roughness was calculated with value of 4.1nm. The height of GST-124 surface fluctuates in a range of 10nm. It reveals that the surface of GST-124 is smooth.

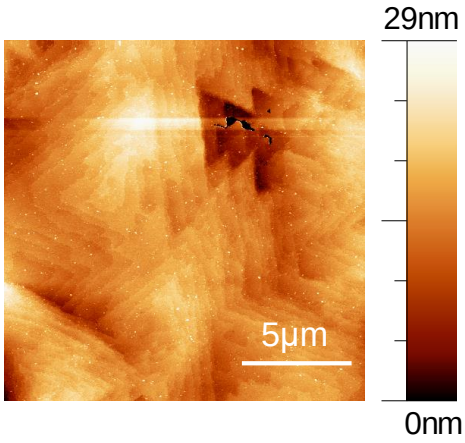

Figure 4.11: AFM characterization of GST-124 grown on Si(111) at 490°C with the applied total gas flow of 3000sccm. The scan area is 15×15 μm^2.

Finally, the lattice parameters of the GST-124 sample were measured by reciprocal space map (RSM) around (1 0 23) reflection of GST-124. The result is depicted in Figure 4.12. Intensity profiles were extracted from the map and are depicted on the top and right-hand side of the picture. The lattice parameters are calculated with values: a=4.35 ± 0.03Å and c=40.6 ± 0.2Å. As revealed, the out-of-plane lattice parameter has a deviation of 0.2Å that might result from the wrong stacks in GST-124 crystals. Not only GST-124 septuple layers exist in the crystals, but also false stacks such as Sb_2Te_3 quintuple layers might insert into the septuple layers.

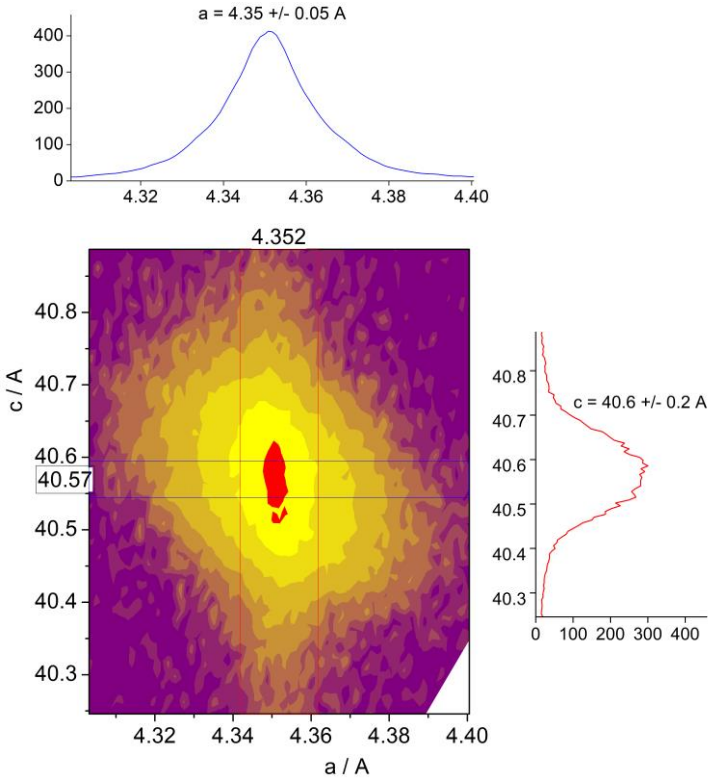

Figure 4.12: Reciprocal space map (RSM) around (1 0 23) reflection of GST-124 deposited at 490°C with the total gas flow of 3000sccm. (RSM performed by Dr. Gregor Mussler and Dr. Alexander Shkurmanov)

In order to improve the precision of the lattice parameter, it was calculated by the equation (4.1). Figure 4.13 presents the XRD results of GST-124 and the relationship diagram between $\sin(\theta I)$ and index.

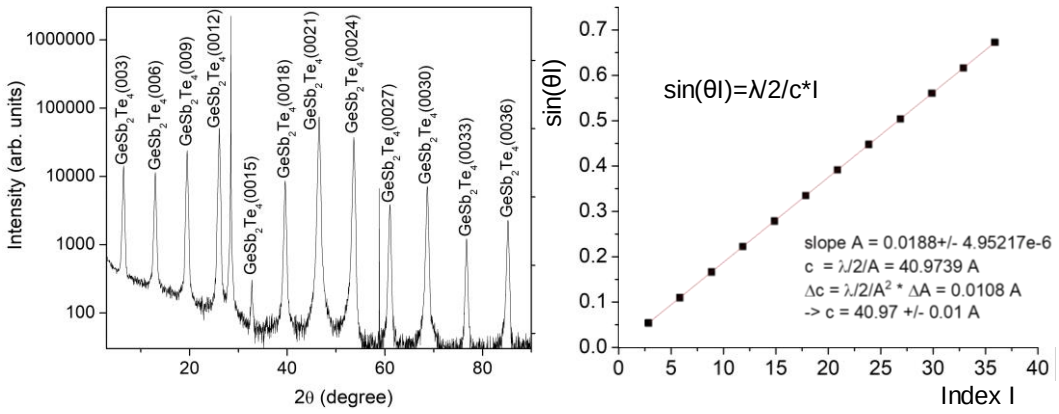

Figure 4.13: Left: XRD image of GST-124. Right: The relationship diagram between $\sin(\theta I)$ and index. (XRD performed by Dr. Gregor Mussler and Dr. Alexander Shkurmanov)

The out-of-plane lattice parameter was calculated with value: c=40.97 ± 0.01Å. However, the in-plane lattice parameter can not be determined by this method.

According to the two methods, the experimental lattice parameters were measured with the values: a=4.35 ± 0.03Å, c=40.97 ± 0.01Å. They differ slightly from the values reported in the literature: a=4.24Å, c=41.12Å [25]. Compared to the theoretical lattice constants, the in-plane lattice parameter is larger, while the out-of-plane lattice parameter is smaller. The discrepancy from the theoretical value suggests an in-plane tensile strain, which is not expected as vdW crystals grow fully relaxed independent of the substrate.

As revealed by the characterization results, GST-124 sample with high quality was realized at the growth temperature of 490°C with the total gas flow of 3000sccm. These parameters can be ultilized as the base to grow GST-147 by reducing Ge flow or increasing the growth temperature.

4.5 Epitaxial growth of stoichiometric state GST-147

This section focuses on epitaxial growth of GST-147. It is a stoichiometric state between Sb_2Te_3 and GST-124. The ratio of Ge in GST-147 is higher than that in Sb_2Te_3, but lower than that in GST-124. In order to grow GST-147, one attempt is increasing Ge flow based on the parameters used for Sb_2Te_3, and then optimizing the growth temperature.

Tab. 4.6: The process and parameters used for epitaxial growth of GST-147.

	Annealing	**Cooling**	**Pretreatment**	**Break**	**Growth**
t/min	28+2	11	2	2	30
Carrier gas	H_2	N_2			
Precursors	DETe	--	Ge_2H_6 , TESb	--	Ge_2H_6 , DETE , TESb
T/℃	690	decrease	475-495		
P/mbar	50				
TGF/sccm	2600	2200	2600	2200	3000

The process and parameters applied to grow GST-147 are depicted in Tab. 4.6. In this section, the total gas flow is kept constant at 3000sccm. Accordingly, the flow of TESb is applied at 192.4sccm, and the flow of DETe is kept with 299.3sccm. Ge_2H_6 flow is explored as the first variable parameter, which varies from 2sccm to 18sccm. The growth temperature is explored as the second variable parameter varing from 475°C to 495°C.

4.5.1 The influence of Ge_2H_6 flow on GST-147

In this section, the epitaxial growth of GST-147 is studied by changing Ge_2H_6 flow from 2sccm to 18sccm. The growth temperature is kept constant with 475°C.

The SEM images of GST samples deposited with different Ge_2H_6 flows are depicted in Figure 4.14. When Ge_2H_6 flow was applied from 6sccm to 18sccm, the GST thin films are coalesced on the substrates. With an increased Ge_2H_6 flow, trigonal steps can be seen on the samples, and the surface is becoming rougher.

However, with the applied Ge_2H_6 flow of 2sccm, only few islands exist on the Si substrates. It's estimated that two reasons could lead to this phenomenon.

- Reason 1: Ge_2H_6 flow is so low that the coalesced GST thin films can not be formed on Si substrate.
- Reason 2: The trigonal islands are formed from the parasitic deposition in the reactor [25], not from the precursors.

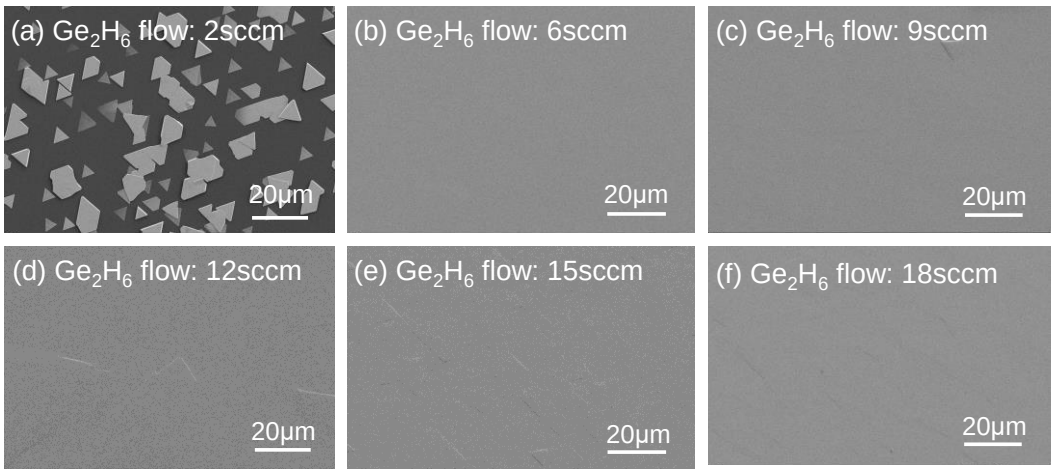

Figure 4.14: SEM images of GST samples grown on Si(111) with different Ge_2H_6 flows at the growth temperature of 475°C. From (a) to (f), the Ge_2H_6 flow changes from 2sccm to 18sccm.

In order to ensure the compositions of the GST samples, they were characterized with XRD. The XRD images are depicted in Figure 4.15. From top to bottom, Ge_2H_6 flows vary from 18sccm to 2sccm.

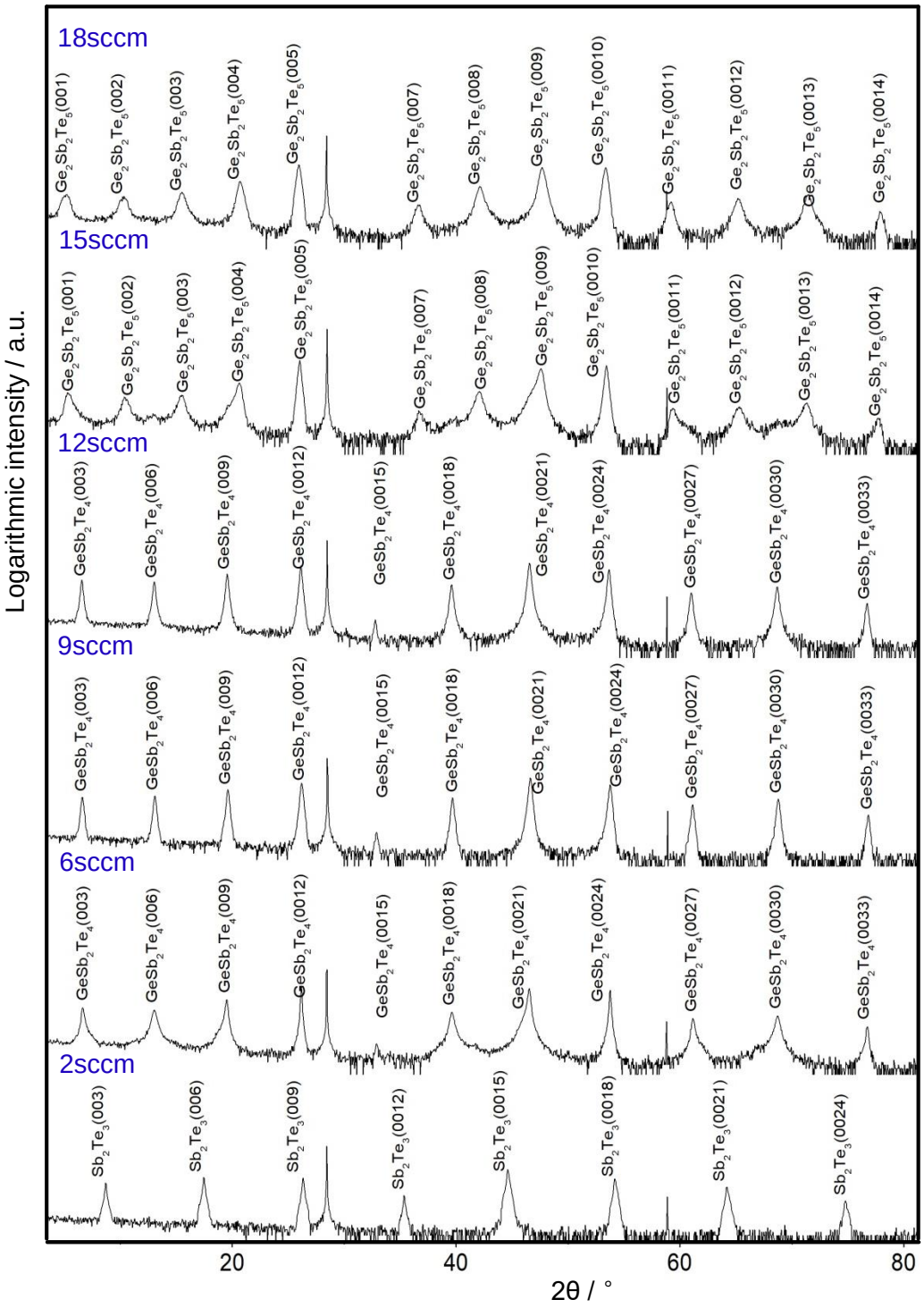

Figure 4.15: XRD images of GST samples grown on Si(111) with different Ge_2H_6 flows at 475°C. From top to bottom, the Ge_2H_6 flow reduces from 18sccm to 2sccm. (XRD performed by Dr. Alexander Shkurmanov)

For the lowest applied Ge_2H_6 flow of 2sccm, this sample is composed of Sb_2Te_3. The result indicates ternary GST alloys can not be grown with a low Ge_2H_6 flow. At 6sccm, the composition of GST-124 was found in the sample. From 6sccm to 12sccm, it reveals no compositional difference in the GST samples. All of them are composed of GST-124. From 15sccm and 18sccm, the composition shifts to GST-225.

In last section, it has been discussed that the ratio of Ge in GST reduces with an increased growth temperature. In order to grow GST-147, the growth temperature can be increased with the applied Ge_2H_6 flow of 6sccm.

4.5.2 The influence of the growth temperature on GST-147

In this section, the Ge_2H_6 flow of 6sccm is applied to grow GST alloys. The total gas flow is kept at 3000sccm. The growth temperature is investigated as the variable parameter from 475°C to 495°C with 5°C step.

The SEM images of GST samples with different growth temperature are depicted in Figure 4.16. At 475°C and 485°C, the surface of the samples is smooth and uniform. However, the surface of the sample grown at 480°C is abnormally rough. It might result from the contamination on the substrate or in the reactor. However, it does not affect the epitaxial growth of GST-147. With an increased growth temperature, some steps in form of fish scales appeared on the surface. It is becoming rougher.

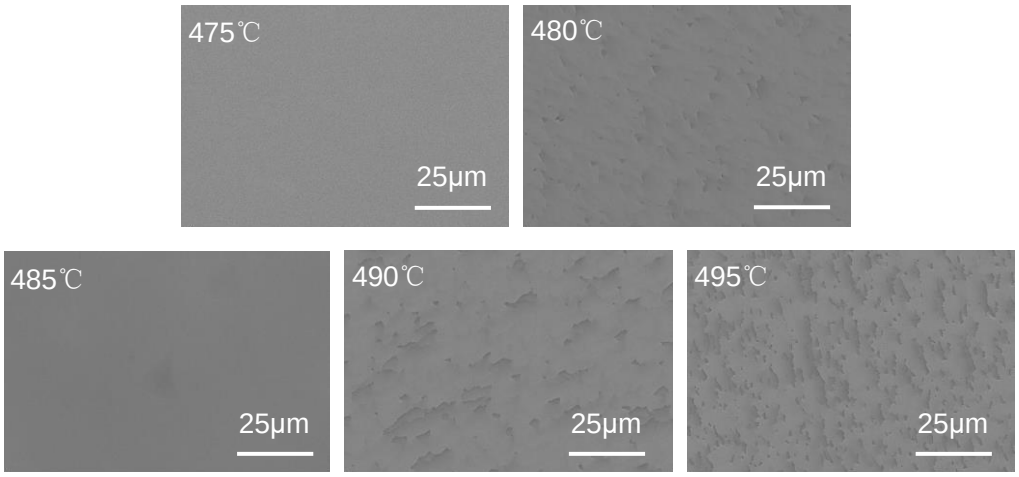

Figure 4.16: SEM images of GST samples grown on Si(111) from 475°C to 495°C with 5°C step. Ge_2H_6 flow is applied with 6sccm. The total gas flow is kept at 3000sccm.

Afterwards, the samples were measured by XRD to analyse their composition. The XRD images of the GST samples grown from 475°C to 495°C are depicted in Figure 4.17.

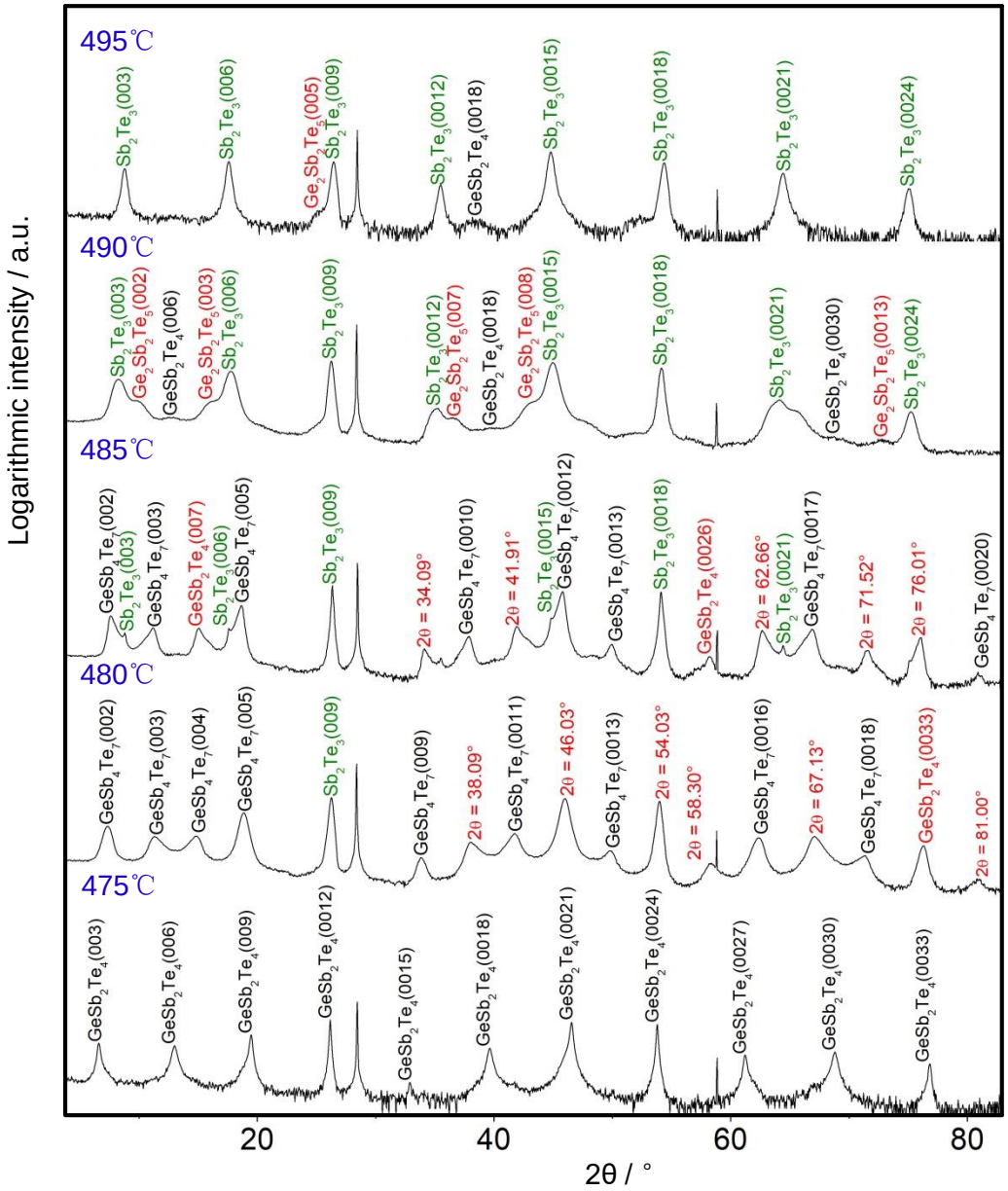

Figure 4.17: XRD images of GST samples grown on Si(111). From top to bottom, the growth temperature changes from 495°C to 475°C. The Ge_2H_6 flow is kept constant at 6sccm. (XRD performed by Dr. Alexander Shkurmanov)

At the lowest applied growth temperature of 475°C, the GST sample is composed of GST-124. An increased growth temperature results in the reduction of Ge ratio

in GST alloys (discussed in section 4.4.1). At 480°C and 485°C, the composition of GST-147 is found in the samples, but not pure. It is composed of a mixture of GST-147 and other phases. At 480°C, the ratio of Ge in GST sample is a little higher than that in pure GST-147 sample, while at 485°C it is a little lower than that in pure GST-147 sample. In order to get pure GST-147, it is necessary to optimize the growth temperature from 480°C to 485°C. The results are discussed in the next section.

4.5.3 Epitaxial growth of GST-147 from 482°C to 484°C

This section focuses on the optimization of the growth temperatures. The growth temperature is controlled as the variable parameter, which is varied from 482°C to 484°C with 1°C step. The total gas flow is kept at 3000sccm. And the Ge_2H_6 flow is kept at 6sccm.

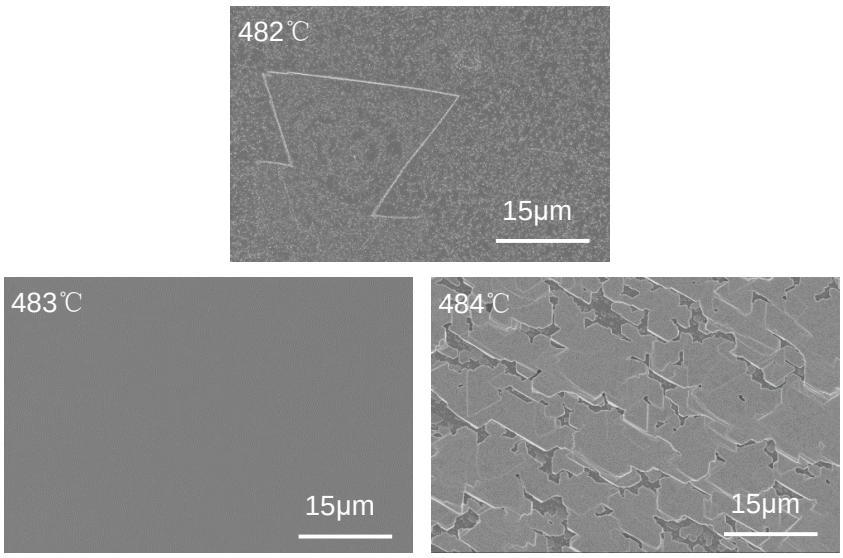

Figure 4.18: SEM images of GST samples grown on Si(111) from 482°C to 484°C. The Ge_2H_6 flow is kept at 6sccm. The total gas flow is kept at 3000sccm.

Firstly, the samples were scanned by SEM to measure their surface topography. The SEM images of GST samples deposited from 482°C to 484°C are depicted in Figure 4.18. With the applied growth temperature of 482°C, trigonal islands are obvious on the surface. At 483°C, the surface of the sample is smooth. However, at 484°C, the steps in form of fish scales formed on the surface. The sample is very rough.

In order to investigate the composition of the samples, they were measured with XRD. The results of the samples are depicted in Figure 4.19. At 482°C, the

sample is composed of a mixture of GST-147 and GST-124. At 483°C, only the phase of GST-147 was found in the sample. At 484°C, the composition of the sample has no big difference from the sample grown at 483°C.

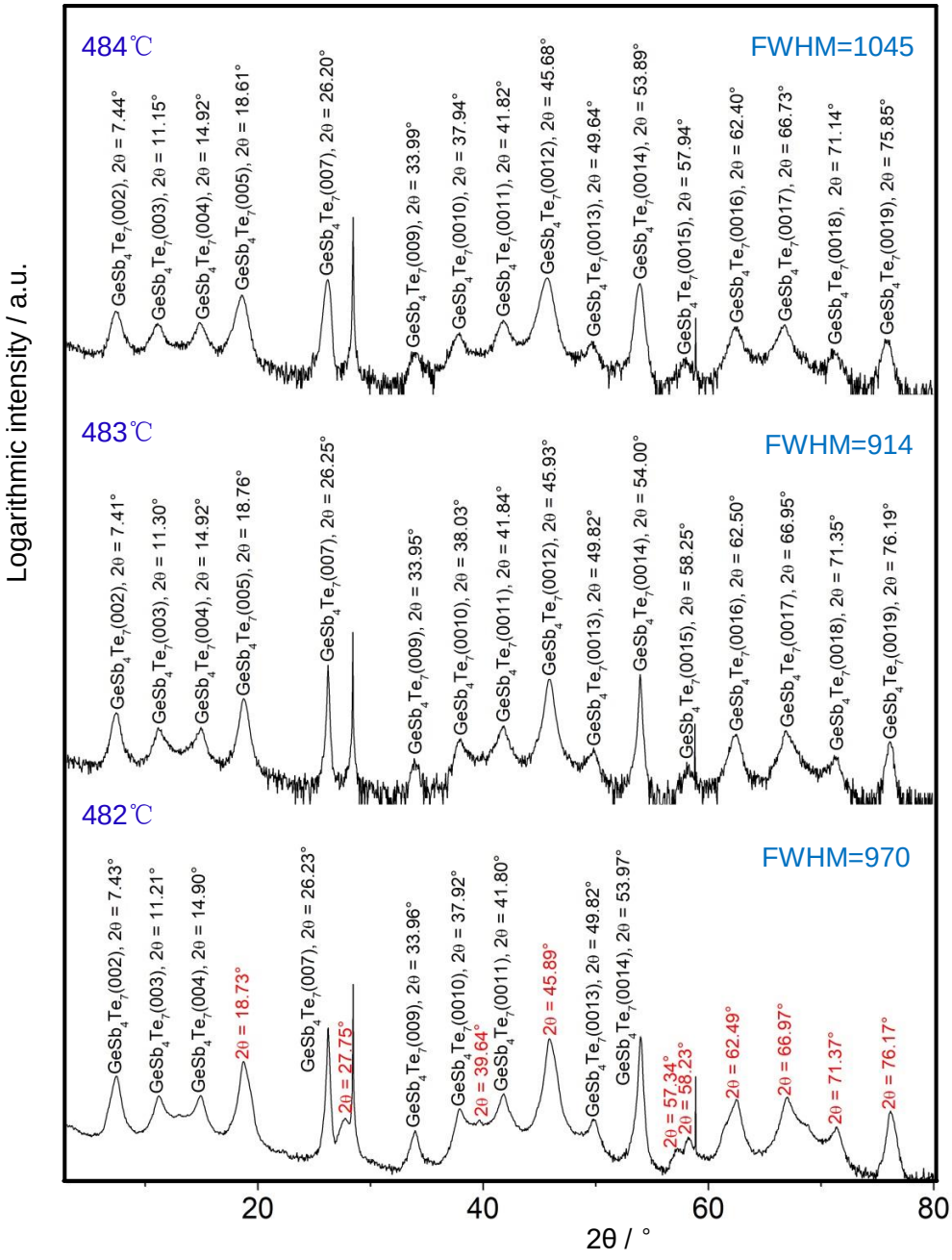

Figure 4.19: XRD images of GST alloys grown on Si(111) at different growth temperatures. From top to bottom, the growth temperature changes from 484°C to 482°C. Rocking curve was measured with GST-147(0012) at around 2θ=46°. (XRD performed by Dr. Alexander Shkurmanov)

The rocking curve of the three samples was measured with the diffraction peak GST-147(0012) at around 2θ=46°. FWHM values are depicted in the XRD images. At 483°C, FWHM was measured with value of 914, which is lower than the value 1045 of the sample grown at 484°C. It confirms that the sample grown at 483°C has the best quality. Its quality can be further researched by AFM, phi-scan, and RSM.

4.5.4 Characterization by AFM, phi-scan, and RSM

In order to calculate the roughness of sample grown at 483°C, it was scanned by AFM with a scan area 15×15 μm^2. The result is depicted in Figure 4.20. RMS roughness of the GST-147 sample was calculated with value 1.69nm. The height of GST-147 surface fluctuates in a range of 5nm. It reveals that the surface topography of the sample has a high quality.

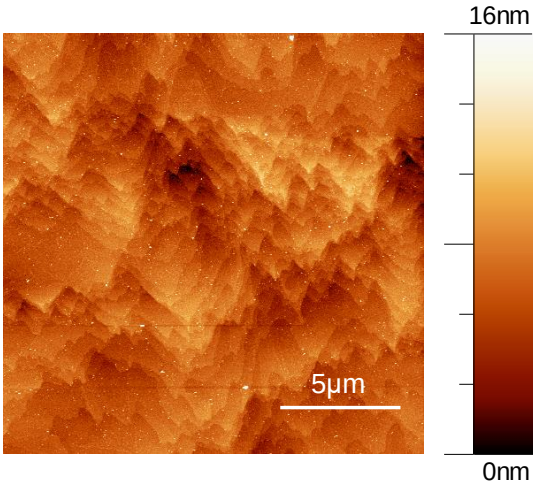

Figure 4.20: AFM characterization of GST-147 grown on Si(111) at the growth temperature of 483°C. The scan area is 15×15 μm^2.

GST alloys have trigonal structure, while Si substrate has hexagonal structure. Therefore, twin domains of GST are formed in the samples. In order to measure the twin domains in the crystal, the sample is tested by phi-scan around (107). The result is depicted in Figure 4.21. As revealed, twin domains exist in the crystal. The ratio of rotational twin domains is around 1:9. The quality of the sample can still be improved.

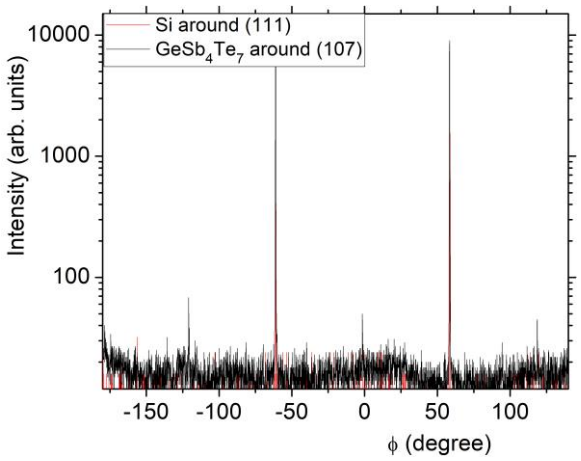

Figure 4.21: Phi-scan around (107) of GST-147 deposited at 483°C. (Phi-scan performed by Dr. Alexander Shkurmanov)

Finally, the lattice parameters were measured by reciprocal space map (RSM) around (1 0 23) reflection of GST-147. The result is depicted in Figure 4.22. Intensity profiles were extracted from the map and are depicted on the top and right-hand side of the picture. The lattice constants are calculated with values: a=4.37 ± 0.01Å and c=23.5 ± 0.3Å.

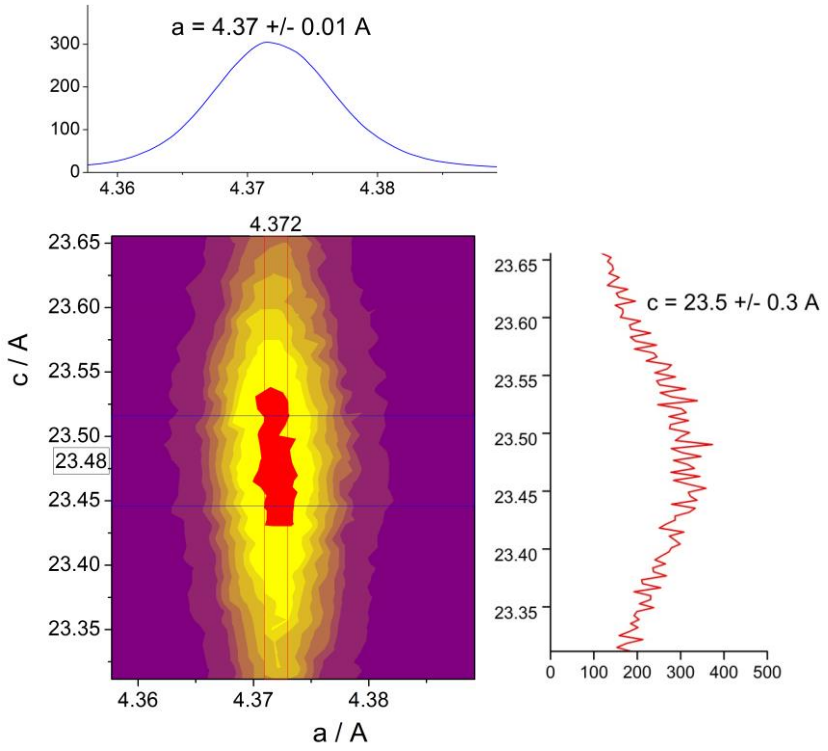

Figure 4.22: Reciprocal space map (RSM) around (1 0 23) reflection of GST-147. (RSM performed by Dr. Gregor Mussler and Dr. Alexander Shkurmanov)

As revealed, the out-of-plane lattice parameter has an obvious deviation of 0.3Å that might result from the wrong stacks in GST-147 crystals. Sb_2Te_3 quintuple layers and GST-124 septuple layers might not alternately form in the crystal.

In order to improve the precision of the out-of-plane lattice parameter, it can also be calculated with equation (4.1). Figure 4.23 presents the XRD image of GST-147 deposited at 483°C and the relationship diagram between $\sin(\theta \mathrm{I})$ and index. The out-of-plane lattice parameter was calculated with value: c=23.77±0.02Å. However, the in-plane lattice parameter can not be determined by this method.

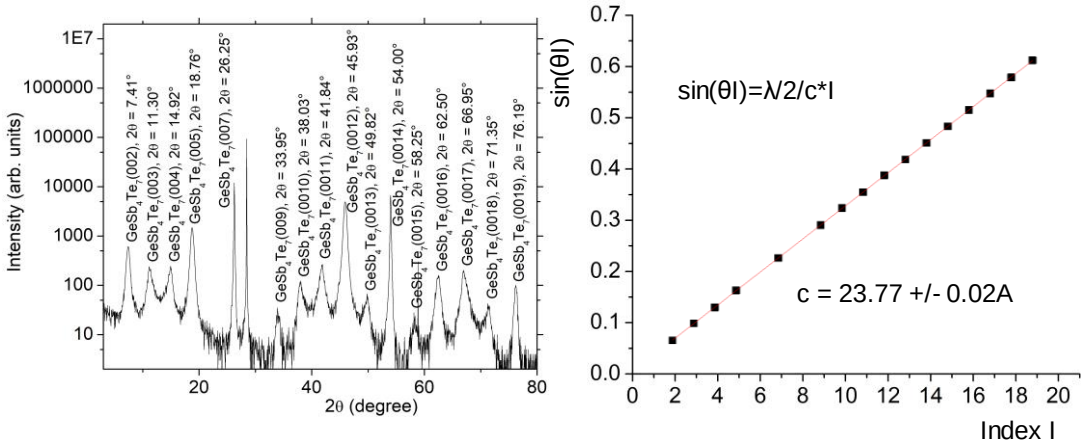

Figure 4.23: XRD image of GST-147 deposited at 483°C and the calculation of the out-of-plane lattice parameter. (XRD performed by Dr. Gregor Mussler and Dr. Alexander Shkurmanov)

According to the two methods, the experimental lattice parameters were measured with the values: a=4.37 ± 0.01Å, c=23.77 ± 0.02Å. They differ slightly from the values reported in the literature: a=4.25Å, c=23.85Å [2]. Compared to the theoretical lattice constants, the in-plane lattice parameter is larger, while the out-of-plane lattice parameter is smaller. The discrepancy from the theoretical value suggests an in-plane tensile strain, which is not expected as vdW crystals grow fully relaxed independent of the substrate.

4.6 Influence of bake-out and substrates quality on GST alloys

Except the growth temperature and the the total gas flow, epitaxial growth of GST alloys can also be influenced by several factors, such as bake-out of the reactor, the quality of the substrates, and the fluctuation of the growth temperature. As discussed, the growth temperature influences the composition and surface

topography of GST alloys. However, it fluctuates within 1°C during epitaxy. This problem can not be avoided. But, the quality of the sample can be improved by repetition of epitaxial growth. This section focuses on the influence of bake-out and substrates quality on the epitaxial growth of GST alloys.

4.6.1 The influence of bake-out on GST alloys

Bake-out is a process of thermal cleaning to remove the parasitic deposition in the reactor. This section investigates the effect of bake-out on GST alloys. The growth temperature is controlled as the variable parameter varing from 481°C to 484°C. The total gas flow is kept at 3000sccm. And the Ge_2H_6 flow is kept at 6sccm. The only difference is that the reactor is not baked out before epitaxy.

Firstly, the samples were scanned by SEM to measure the coalescence of the thin films. The SEM images of the samples are depicted in Figure 4.24. With the applied growth temperature of 481°C, 482°C, and 483°C, the thin films are coalesced on the substrates. The surfaces are very smooth. At 484°C, the steps in form of fish scales were formed on the surface. Compared to the SEM images in Figure 4.18, the surface topography of the samples has no difference.

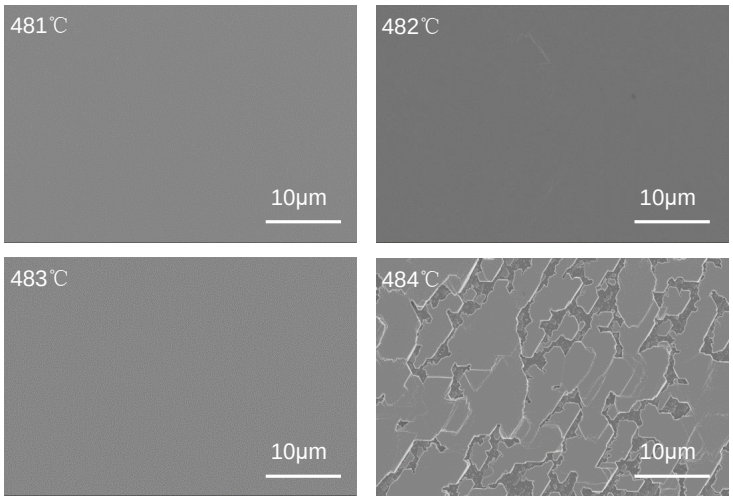

Figure 4.24: SEM images of GST samples grown on Si(111) from 481°C to 484°C. The Ge_2H_6 flow is kept at 6sccm. The total gas flow is kept at 3000sccm. Before epitaxy, the reactor was not baked out.

Afterwards, the composition of the samples is measured by XRD. The XRD images are depicted in Figure 4.25. As revealed, all of the four samples are composed of a mixture phase. Pure GST-147 phase was not found in the

samples. Compared to the samples in Figure 4.19, bake-out influences the composition of the samples.

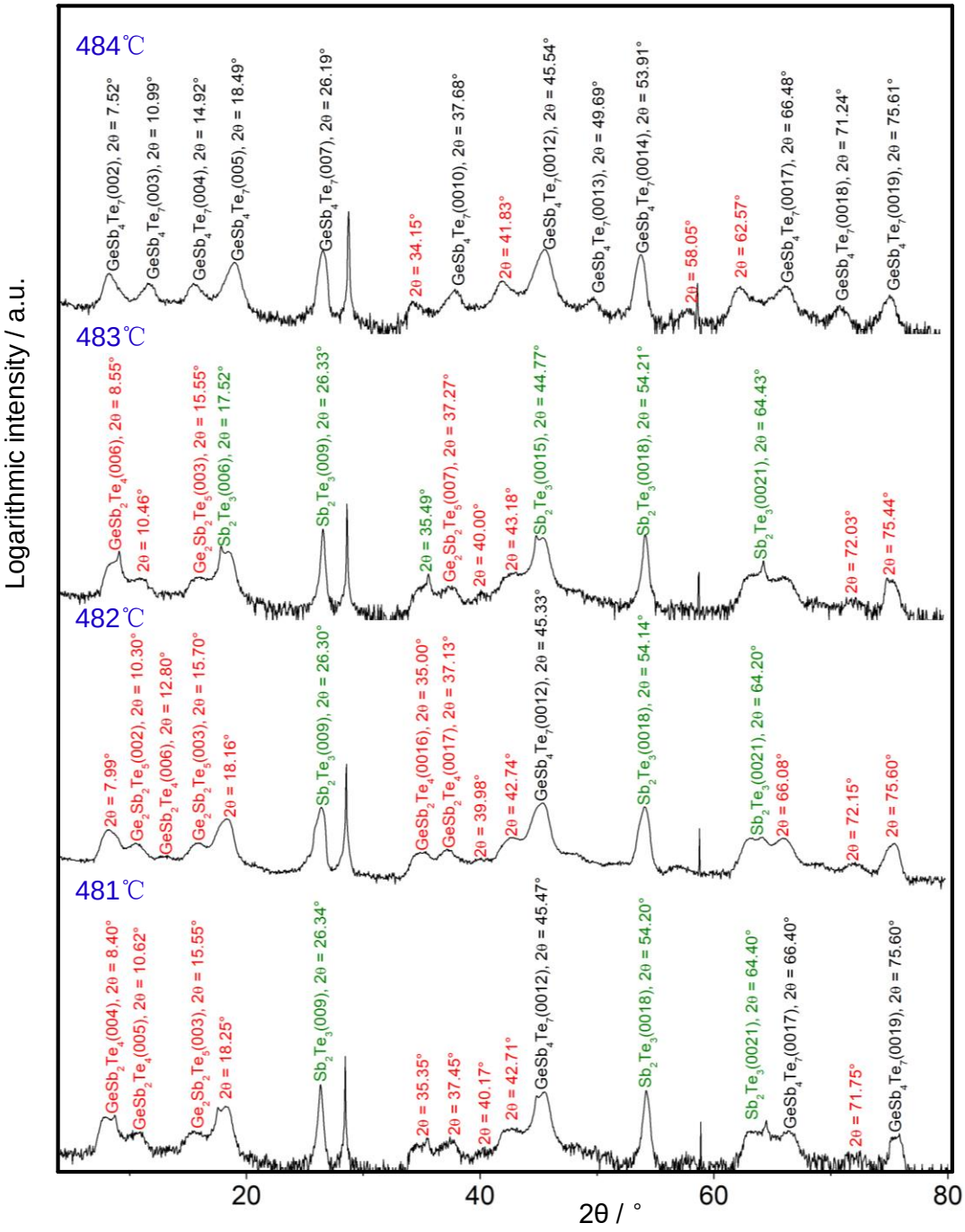

Figure 4.25: XRD images of GST samples grown on Si(111) with different growth temperatures. From top to bottom, the growth temperature changes from 484°C to 481°C. Before epitaxy, the reactor was not baked out. (XRD performed by Dr. Alexander Shkurmanov)

Compared to the results of last section, bake-out does not influence the surface topography of GST samples. However, it affects the composition of the samples, as parasitic deposition exists in the reactor.

4.6.2 Influence of substrates quality on GST alloys

In this section, the effects of substrates quality on the samples are discussed. The main flaw of the substrates is miscut. In order to investigate the influence of substrates quality, comparative experiments were set up. In the first group, Si wafers with high quality are utilized to deposit GST-147 thin films. In the second group, GST-147 samples are grown on miscut Si substrates, which were measured with the values: at 2θ=0°, Zeta1=-0.610998 and Xi1=-0.03666, at 2θ=28.44°, Zeta2=0.8700 and Xi2=0.015004. The miscut is about 0.9°.

As revealed in section 4.5.3, the GST-147 sample deposited at 483°C is the best one. In this part, growth temperature of 483°C is also applied to deposit GST alloys. Other growth parameters are kept the same as that in chapter 4.5.3.

Firstly, the surface topography of the samples was measured and compared. The SEM images of GST samples deposited at 483°C are depicted in Figure 4.26. The left sample was grown on Si(111), while the right sample was deposited on miscut Si(111). As shown, it formed steps on miscut Si wafers. However, the thin film is smooth on Si wafers with high quality.

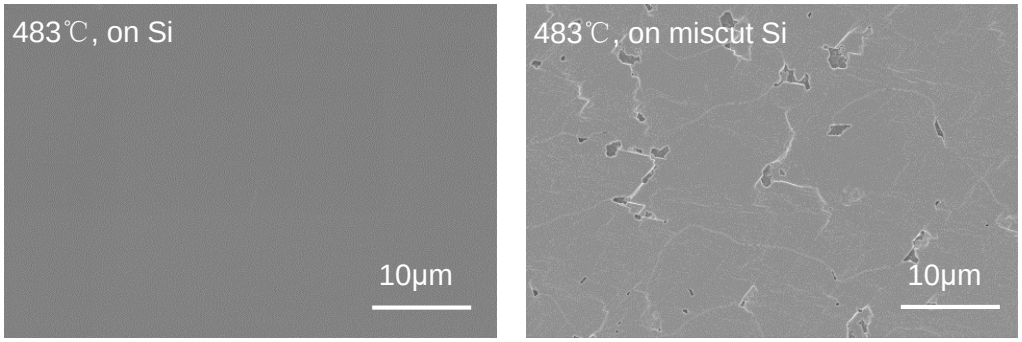

Figure 4.26: SEM images of GST alloys deposited at 483°C. Left: Epitaxy on Si(111). Right: Epitaxy on miscut Si(111).

Afterwards, the composition of the samples was investigated by XRD. The XRD images of the GST alloys grown at 483°C are depicted in Figure 4.27. The left image indicates the composition of the sample grown on Si with high quality. It is composed of GST-147. The right image indicates the composition of the sample deposited on miscut Si substrate. It is also composed of GST-147. The

compositions of the GST samples have no difference. In addition, the rocking curve was measured with the diffraction peak GST-147(0012). As revealed, the two samples have almost the same FWHM values.

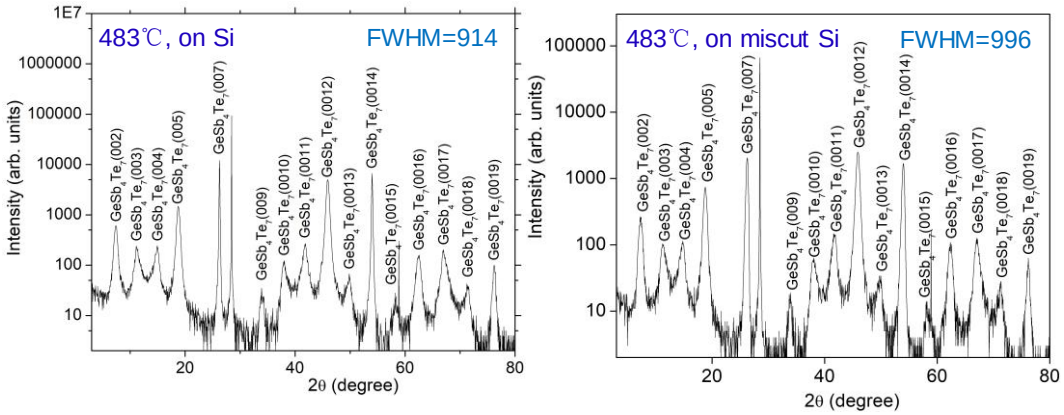

Figure 4.27: XRD images of the GST alloys grown at 483°C. Left: Deposition of GST on Si(111). Right: Deposition of GST on miscut Si(111). (XRD performed by Dr. Alexander Shkurmanov)

It can be seen, the quality of the substrates influences the surface topography of GST samples. However, it does not affect the composition of GST alloys.

4.7 Summary

In this chapter, pure Sb_2Te_3, GST-124, and GST-147 have been successfully grown on Si(111) via MOVPE. Before epitaxy, the reactor must be thermally cleaned with H_2 to remove contaminations on the wafers and in the reactor. And the substrate is treated by Te precursor to deposit one layer Te atoms, which help vdW-epitaxy. The parameters affecting the epitaxial quality have been studied in great details. The effects of the growth temperature, the total gas flow, and the flow of individual precursors have been studies in detail. The growth temperature influences not only the surface topography of the samples, but also the composition of the thin films. With a higher applied growth temperature, the ratio of Ge in GST alloys reduces. The total gas flow has little influence on the surface topography and the composition of the samples. By adjusting the flow of individual precursors and the substrates temperature, tuning of the stoichiometric states can be realized.

5 Epitaxial growth of stoichiometric GST alloys via MBE

The epitaxial growth of GST alloys via MOVPE has been discussed in chapter 4. By adjusting the total gas flow, the growth temperature, and the flow of individual precursors, the target can be achieved. The epitaxial growth via MBE can also be realized by adjusting the substrates temperature and the temperature of individual effusion cells. My colleague Abdur Rehman Jalil has discussed it in detail. In my thesis, the point was shifted to the selective area epitaxy (SAE) of GST alloys.

5.1 Selective area epitaxy (SAE)

Selective area epitaxy (depicted in Figure 5.1) is a technique utilized for epitaxial growth of crystals only on desired areas. In order to realize selective area epitaxy, a blocking surface is firstly fabricated on Si(111). Afterwards, the blocking surface is developed by lithography and etching to complete the pre-patterned substrates. The epitaxial growth happens on the area without blocking surface.

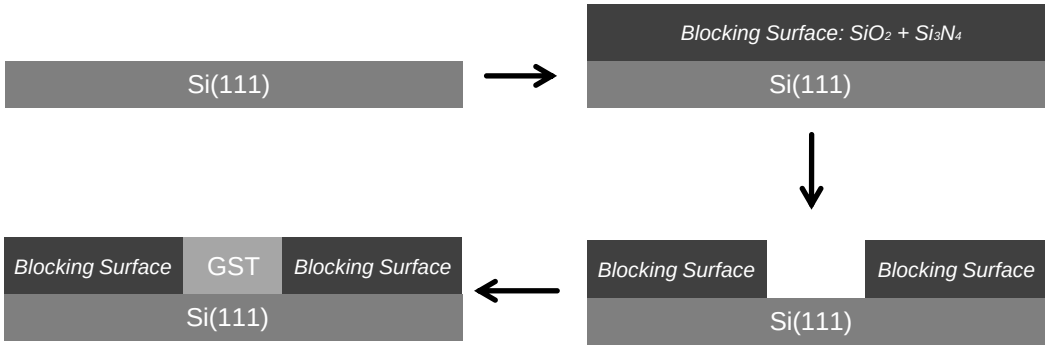

Figure 5.1: Selective area epitaxy (SAE) of GST alloys on Si(111) substrates. (SAE substrate fabrication performed by Abdur Rehman Jalil)

5.1.1 SAE of GST alloys

The first attempt is SAE of Sb_2Te_3 on Si(111) via MBE. In order to apply Sb_2Te_3 to nanostructures, Sb_2Te_3 was grown on 500nm wide hall bar for 4 hours via MBE. The SEM images of selective area epitaxy of Sb_2Te_3 on Si(111) are depicted in Figure 5.2. The darker area represents the blocking surface of SiN_X, while the lighter area is the Sb_2Te_3 deposited on Si(111).

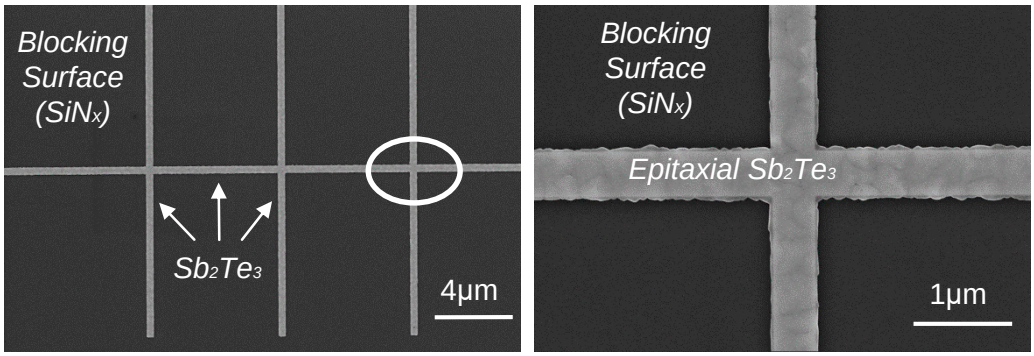

Figure 5.2: SEM images of selective area epitaxy of Sb_2Te_3 on pre-patterned Si(111). Both of the two images indicate SAE of 500nm wide hall bars. The right image is the enlargement of the cross in the first image. The darker area represents the blocking surface of SiN_X, while the lighter area is Sb_2Te_3 deposited on Si(111).

The second attempt is to fabricate GST nanostructures via MBE. The GST alloys were deposited on 1500nm wide hall bar with much wider contacting lines for 4 hours. The SEM images of selective area epitaxy of GST alloys on pre patterned Si(111) are depicted in Figure 5.3. The darker area represents the blocking surface of SiN_X, while the lighter area is the GST thin film deposited on Si(111).

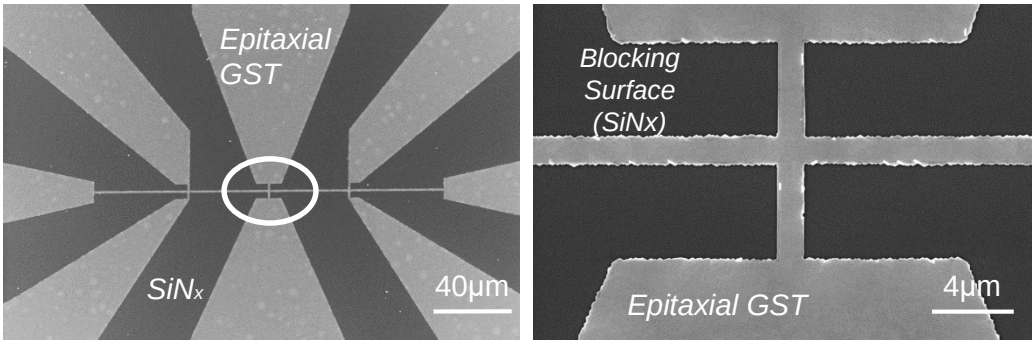

Figure 5.3: SEM images of selective area epitaxy of GST on pre-patterned Si(111). The two images show SAE of 1500nm wide hall bars with much wider contacting lines. The right image is the enlargement of the circle in the first image. The darker area represents the blocking surface of SiN_X, while the lighter area is GST alloy deposited on Si(111).

5.1.2 Influence factors of SAE

Selective area epitaxy can be influenced by several factors:

- The substrates temperature

- The quality of the substrates
- Growth dynamics

A lower substrates temperature leads to the failure of SAE. With a low applied temperature, GST alloys grow not only on the pre-patterned areas, but also on the blocking surface. The result is depicted Figure 5.4. With a higher applied substrates temperature, GST alloys do not grow on the substrates. In addition, the quality of the substrates must be very high. The comtaminations on the substrate destroy the nanostructures.

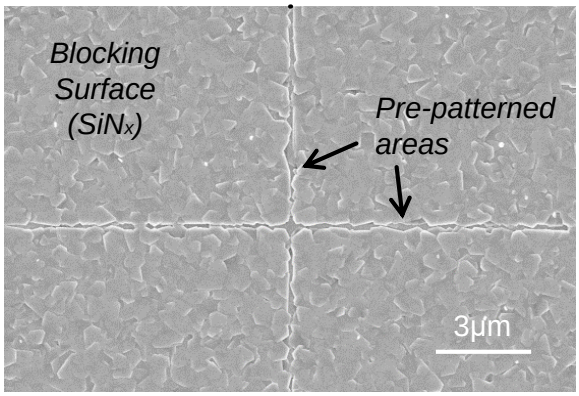

Figure 5.4: Selective area epitaxy of GST on pre-patterned Si(111) with a lower substrates temperature.

The growth dynamics has also a big influence on SAE. When the growth rate is much higher than the rate on planar substrates, over-growth (depicted in Figure 5.5) happens. However, it depends on the dimension of the patterns. Over-growth happens more easily on the nanostructures with a small dimension.

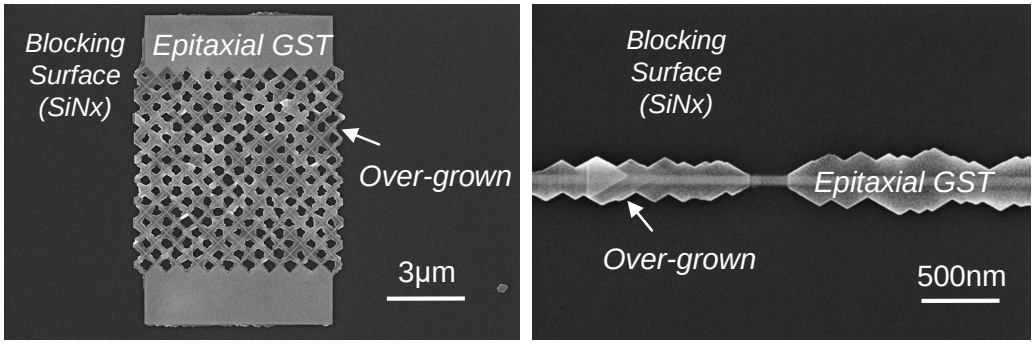

Figure 5.5: Over-grown of SAE. The darker area represents the blocking surface of SiN_X, while the lighter area is GST alloys deposited on Si(111).

5.1.3 Advantages of SAE

Selective area epitaxy has many advantages:

- Fabricate nanostructures in-situ without exposing to air [56].
- Scalable and reproduceable technique.
- Possibly incorporated into fabrication industry.

5.2 Comparison of MOVPE and MBE

The epitaxial growth of stoichiometric GST alloys via MOVPE and MBE has been discussed. This section focuses on the comparison of MOVPE and MBE. The two epitaxial methods have their own advantages and disadvantages.

Growth parameters

- The epitaxy via MBE is controlled by the temperature of effusion cells and the growth temperature.
- In MOVPE system, the deposition is controlled by the growth temperature, the total gas flow, the flow of precursors, and the pressure of the reactor. The variable parameters in MOVPE system are more complicated.

Deposition rate

- The epitaxial growth via MOVPE is much quicker than via MBE. It took about 30 to 60min to deposit one sample via MOVPE. And the thickness is around 200nm.
- However, it took 4 hours to grow one sample via MBE. The thickness of samples is 40nm.

Quality of the samples

- The surface topography of the samples grown via MBE is a little better than via MOVPE.
- The roughness of the samples deposited via MBE is a little smaller than via MOVPE.

Selective area epitaxy

- Selective area epitaxy of GST alloys has been realized by MBE.
- SAE via MOVPE is still under progress.

6 Conclusion and Outlook

The epitaxial growth on Si(111) has been successfully achieved. The growth mechanism of the thin films via MOVPE is understood. By MOVPE, three different stoichiometric states (Sb_2Te_3, GST-124, and GST-147) of phase-change materials have been achieved.

The parameters affecting the samples quality have been studied in great detail. The influence of the growth temperature, the total gas flow, and the flow of individual precursors on the structural quality has been successfully investigated. SEM and AFM results indicated the samples have good surface topography. XRD investigation has shown that the crystals have high quality. RSM results show the lattice parameters match the literature, although small variations have been found. They might result from the presence of wrong stacks in the crystals.

The same GST stoichiometric states have been grown via MBE. In this thesis, the point was shifted to the selective area epitaxy. In order to realize selective area epitaxy, the wafer was covered by the blocking surface made of SiO_2 and Si_3N_4, and then developed to complete pre-patterned substrates. With the help of the substrates temperature and the individual beam flux, the growth rate can be controlled to achieve SAE in the three patterned substrates on Si(111).

In the future, the same substrates can be utilized to optimize the SAE via MOVPE. And the nanostructures can be fabricated to be used for CMOS fabrication.

Outlook

- To achieve selective area epitaxy via MOVE of the desired stoichiometric states of GST alloys.
- Tune the stoichiometric states, until they can be utilized to achieve iPCM for lower power applications.
- Tune and achieve epitaxial growth of pure GeTe. The epitaxy is a challenge. With the help of GeTe, SAE and lots of applications will become accessible.

7 References

[1] R. E. Simpson, P. Fons, a. V. Kolobov, T. Fukaya, M. Krbal, T. Yagi, and J. Tominaga, "Interfacial phase-change memory," Nature Nanotechnology, vol. 6, p. 501, jul 2011.

[2] http://www2.fiz-karlsruhe.de, "ICSD - Inorganic Crystal Structure Database," accessed August 22, 2020.

[3] M. Wuttig and N. Yamada, "Phase-change materials for rewriteable data storage," Nature Materials, vol. 6, no. 11, p. 824, 2007.

[4] T. Ohta, K. Nishiuchi, K. Narumi, Y. Kitaoka, H. Ishibashi, N. Yamada, and T. Kozaki, "Overview and the Future of Phase-Change Optical Disk Technology," Japanese Journal of Applied Physics, vol. 39, no. 2B, p. 770, 2000.

[5] D. Lencer, M. Salinga, B. Grabowski, T. Hickel, J. Neugebauer, and M. Wuttig, "A map for phase-change materials," Nature Materials, vol. 7, no. 12, p. 972, 2008.

[6] M. Schuck, S. Rieß, M. Schreiber, G. Mussler, D. Grützmacher, and H. Hardtdegen, "Metal organic vapor phase epitaxy of hexagonal Ge-Sb-Te (GST)," Journal of Crystal Growth, vol. 420, p. 37, 2015.

[7] J. L. F. Da Silva, A. Walsh, and H. Lee, "Insights into the structure of the stable and metastable $(GeTe)_m(Sb_2Te_3)_n$ compounds," Physical Review B, vol. 78, no. 22, p. 224111, 2008.

[8] T. Matsunaga and N. Yamada, "Structural investigation of $GeSb_2Te_4$: A high-speed phase-change material," Physical Review B, vol. 69, no. 10, p. 104111, 2004.

[9] T. Nonaka, G. Ohbayashi, Y. Toriumi, Y. Mori, and H. Hashimoto, "Crystal structure of GeTe and $Ge_2Sb_2Te_5$ meta-stable phase," Thin Solid Films, vol. 370, no. 1, p. 258, 2000.

[10] H.-S. Wong, S. Raoux, S. Kim, J. Liang, J. P. Reifenberg, B. Rajendran, M. Asheghi, and K. E. Goodson, "Phase Change Memory," Proceedings of the IEEE, vol. 98, no. 12, p. 2201, 2010.

[11] X. S. Miao, L. P. Shi, H. K. Lee, J. M. Li, R. Zhao, P. K. Tan, K. G. Lim, H. X. Yang, and T. C. Chong, "Temperature Dependence of Phase-Change Random Access Memory Cell," Japanese Journal of Applied Physics, vol. 45, no. 5A, p. 3955, 2006.

[12] F. Bedeschi, R. Bez, C. Boffino, E. Bonizzoni, E. Buda, G. Casagrande, L. Costa, M. Ferraro, R. Gastaldi, O. Khouri, F. Ottogalli, F. Pellizzer, A. Pirovano, C. Resta, G. Torelli, and M. Tosi, "4-Mb MOSFET-Selected µTrench Phase-Change Memory Experimental Chip," IEEE Journal of Solid-State Circuits, vol. 40, no. 7, p. 1557, 2005.

[13] L. Okabe, Aditya Sood, Eilam Yalon, Christopher M. Neumann, Mehdi Asheghi, Eric Pop, Kenneth E. Goodson, and H.-S. Philip Wong, "Understanding the switching mechanism of interfacial phase change memory", J. Appl. Phys. 125, 184501 (2019).

[14] N. Takaura, T. Ohyanagi, M. Tai, M. Kinoshita, K. Akita, T. Morikawa, S. Kato, M. Araidani, K. Kamiya, T. Yamamoto, and K. Shiraishi, in Proceedings of the 2014 International Conference on Microelectronic Test Structures (ICMTS), Udine, Italy, 24 March-27 March 2014 (IEEE, 2014), pp. 32-37.

[15] J. Tominaga, A. V. Kolobov, P. Fons, T. Nakano, and S. Murakami, "Ferroelectruc order control of the Dirac-Semimetal phase in GeTe-Sb_2Te_3 superlattices", Adv. Mater. Interfaces 1, 1300027 (2013).

[16] D. Bang, H. Awano, J. Tominaga, A. V. Kolobov, P. Fons, Y. Saito, K. Makino, T. Nakano, M. Hase, Y. Takagaki, A. Giussani, R. Calarco, and S. Murakami, "Mirror-symmetric Magneto-optical Kerr Rotation using Visible Light in $[(GeTe)_2(Sb_2Te_3)_1]_n$ Topological Superlattices", Sci. Rep. 4, 5727 (2014).

[17] J. Tominaga, A. V. Kolobov, P. J. Fons, X. Wang, Y. Saito, T. Nakano, M. Hase, S. Murakami, J. Herfort, and Y. Takagaki, "Giant multiferroic effects in topological GeTe-Sb_2Te_3 superlattices", Sci. Technol. Adv. Mater. 16, 1 (2015).

[18] T. Ohyanagi, M. Kitamura, M. Araidai, S. Kato, N. Takaura, and K. Shiraishi, "GeTe sequences in superlattice phase change memories and their electrical characteristics," Applied Physics Letters, vol. 104, no. 25, p. 2014, 2014.

[19] X. Yu, J. Robertson, "Modeling of switching mechanism in GeSbTe chalcogenide superlattices," Scientific Reports, vol. 5, p. 12612, 2015.

[20] J. Momand, F. R. Lange, R. Wang, J. E. Boschker, M. A. Verheijen, R. Calarco, M. Wuttig, and B. J. Kooi, "Atomic stacking and van-der-Waals bonding in GeTe-Sb_2Te_3 superlattices," Journal of Materials Research, vol. 31, no. 20, p. 3115, 2016.

[21] J. Momand, R. Wang, J. E. Boschker, M. A. Verheijen, R. Calarco, and B. J. Kooi, "Interface formation of two- and three-dimensionally bonded materials in the case of GeTe-Sb_2Te_3 superlattices," Nanoscale, vol. 7, no. 45, p. 19136, 2015.

[22] T. Matsunaga, N. Yamada, and Y. Kubota, "Structures of stable and metastable $Ge_2Sb_2Te_5$, an intermetallic compound in GeTe-Sb_2Te_3 pseudobinary systems," Acta Crystallographica, vol. B60, no. 6, p. 685, 2004.

[23] J. Tominaga, P. Fons, A. Kolobov, T. Shima, T. C. Chong, R. Zhao, H. K. Lee, and L. Shi, "Role of Ge switch in phase transition: Approach using atomically controlled GeTe/Sb_2Te_3 superlattice," Japanese Journal of Applied Physics, vol. 47, no. 7, p. 5763, 2008.

[24] M. Schuck, S. Rieß, M. Schreiber, G. Mussler, D. Grützmacher, and H. Hardtdegen, "Metal organic vapor phase epitaxy of hexagonal Ge-Sb-Te (GST)," Journal of Crystal Growth, vol. 420, p. 37, 2015.

[25] A. Ratajczak, M. von der Ahe, H. Du, G. Mussler, and D. Grützmacher, "Metal organic vapor phase epitaxy of $Ge_1Sb_2Te_4$ thin films on Si(111) substrate," Applied Physics A, vol. 125, p. 163, 2019.

[26] A. C. Jones and M. L. Hitchman, "Overview of Chemical Vapour Deposition," in Chemical Vapour Deposition: Precursors, Processes and Applications, ch. 1, p. 1, Royal Society of Chemistry, 2009.

[27] K. Pu, X. Dai, D. Miao, S. Wu, T. Zhao, and Y. Hao, "A kinetics model for MOCVD deposition of AlN film based on Grove theory," Journal of Crystal Growth, vol. 478, p. 42, 2017.

[28] G. B. Stringfellow, "A critical appraisal of growth mechanisms in MOVPE," Journal of Crystal Growth, vol. 68, no. 1, p. 111, 1984.

[29] R. A. Talalaev, E. V. Yakovlev, S. Y. Karpov, and Y. N. Makarov, "On low temperature kinetic effects in metal-organic vapor phase epitaxy of III-V compounds," Journal of Crystal Growth, vol. 230, no. 1-2, p. 232, 2001.

[30] P. I. Kuznetsov, B. S. Shchamkhalova, V. O. Yapaskurt, V. D. Shcherbakov, V. A. Luzanov, G. G. Yakushcheva, V. A. Jitov, and V. E. Sizov, "MOVPE deposition of Sb_2Te_3 and other phases of Sb-Te system on sapphire substrate," Journal of Crystal Growth, vol. 471, p. 1, 2017.

[31] M. Longo, O. Salicio, C. Wiemer, R. Fallica, A. Molle, M. Fanciulli, C. Giesen, B. Seitzinger, P. K. Baumann, M. Heuken, and S. Rushworth, "Growth study of $Ge_xSb_yTe_z$ deposited by MOCVD under nitrogen for non-volatile memory applications," Journal of Crystal Growth, vol. 310, no. 23, p. 5053, 2008.

[32] G. Bendt, S. Zastrow, K. Nielsch, P. S. Mandal, J. Sanchez-Barriga, O. Rader, and S. Schulz, "Deposition of topological insulator Sb_2Te_3 films by an MOCVD process," Journal of Materials Chemistry A, vol. 2, no. 22, p. 8215, 2014.

[33] O. Karpinsky, L. Shelimova, M. Kretova, and J. P. Fleurial, "An X-ray study of the mixed-layered compounds of $(GeTe)_n(Sb_2Te_3)_m$ homologous series," Journal of Alloys and Compounds, vol. 268, no. 1-2, p. 112, 1998.

[34] J. I. Goldstein, Scanning Electron Microscopy and X-Ray Microanalysis. 3rd ed., 2003.

[35] C. Suryanarayana and M. Grant Norton, X-Ray Diffraction. A Practical Approach, Springer, 1998.

[36] A. Krost, G. Bauer, and J. Woitok, "High Resolution X-Ray Diffraction," in Optical Characterization of Epitaxial Semiconductor Layers, ch. 6, p. 287, Springer, 1996.

[37] R. Perez and R. Garcia, "Dynamic atomic force microscopy methods," Surface Science Reports, vol. 47, no. 6-8, p. 197, 2002.

[38] H. J. Butt, B. Cappella, and M. Kappl, "Force measurements with the atomic force microscope: Technique, interpretation and applications," Surface Science Reports, vol. 59, no. 1-6, p. 1, 2005.

[39] Q. Zhong, D. Inniss, K. Kjoller, and V. B. Elings, "Fractured polymer/silica fiber surface studied by tapping mode atomic force microscopy," Surface Science Letters, vol. 290, no. 1-2, p. L688, 1993.

[40] R. Perez and R. Garcia, "Dynamic atomic force microscopy methods," Surface Science Reports, vol. 47, no. 6-8, p. 197, 2002.

[41] J. I. Goldstein, Scanning Electron Microscopy and X-Ray Microanalysis. 3rd ed., 2003.

[42] https://www.thermofisher.com/blog/, "SEM: Types of Electrons and the Information They Provide," accessed August 28, 2020.

[43] L. Reimer and H. Kohl, Transmission Electron Microscopy: Physics of Image Formation. Springer Verlag, 5th ed., 2008.

[44] R. A. Talalaev, E. V. Yakovlev, S. Y. Karpov, and Y. N. Makarov, "On low temperature kinetic effects in metal-organic vapor phase epitaxy of III-V compounds," Journal of Crystal Growth, vol. 230, no. 1-2, p. 232, 2001.

[45] M. R. Leys and H. Veenvliet, "A study of the growth mechanism of epitaxial GaAs as grown by the technique of metal organic vapour phase epitaxy," Journal of Crystal Growth, vol. 55, no. 1, p. 145, 1981.

[46] G. B. Stringfellow, "A critical appraisal of growth mechanisms in MOVPE," Journal of Crystal Growth, vol. 68, no. 1, p. 111, 1984.

[47] M. Lanius, J. Kampmeier, S. Kölling, G. Mussler, P. M. Koenraad, and D. Grützmacher, "Topography and structure of ultrathin topological insulator Sb_2Te_3 films on Si(111) grown by means of molecular beam epitaxy," Journal of Crystal Growth, vol. 453, p. 158, 2016.

[48] J. Kampmeier, S. Borisova, L. Plucinski, M. Luysberg, G. Mussler, and D. Grützmacher, "Suppressing Twin Domains in Molecular Beam Epitaxy Grown Bi_2Te_3 Topological Insulator Thin Films," Crystal Growth & Design, vol. 15, no. 1, p. 390, 2015.

[49] G. Bendt, S. Zastrow, K. Nielsch, P. S. Mandal, J. Sanchez-Barriga, O. Rader, and S. Schulz, "Deposition of topological insulator Sb_2Te_3 films by an MOCVD process," Journal of Materials Chemistry A, vol. 2, no. 22, p. 8215, 2014.

[50] H. Hardtdegen and P. Giannouls, "MOVPE gets green signal," III-Vs Review, vol. 11, no. 5, p. 34, 1998.

[51] A. Giani, A. Boulouz, F. Pascal-Delannoy, A. Foucaran, E. Charles, and A. Boyer, "Growth of Bi_2Te_3 and Sb_2Te_3 thin films by MOCVD," Materials Science and Engineering B, vol. 64, no. 1, p. 19, 1999.

[52] M. Longo, O. Salicio, C. Wiemer, R. Fallica, A. Molle, M. Fanciulli, C. Giesen, B. Seitzinger, P. K. Baumann, M. Heuken, and S. Rushworth, "Growth study of $Ge_xSb_yTe_z$ deposited by MOCVD under nitrogen for non-volatile memory applications," Journal of Crystal Growth, vol. 310, no. 23, p. 5053, 2008.

[53] A. Koma, "Van der Waals epitaxy: a new epitaxial growth method for a highly lattice-mismatched system," Thin Solid Films, vol. 216, no. 1, p. 72, 1992.

[54] J. E. Boschker, J. Momand, V. Bragaglia, R. Wang, K. Perumal, A. Giussani, B. J. Kooi, and H. Riechert, "Surface Reconstruction-Induced Coincidence Lattice Formation Between Two-Dimensionally Bonded Materials and a Three-Dimensionally Bonded Substrate," Nano Letters, vol. 14, no. 6, p. 3534, 2014.

[55] R. Dittmann, J. P. Strachan, "Redox-based memristive devices for newcomputing paradigm," APL Material 7 (11):110903 (2019).

[56] *Peter Schüffelgen.Exploiting Topological Insulators for Majorana Devices and Physics via Molecular Beam Epitaxy: [D].Aachen: Aachen RWTH university, 2018.*

8 Acknowledgments

During my master thesis in PGI-9, many people helped me a lot. Here, I would like to acknowledge all people who supported me.

First of all, I want to thank Prof. Dr. Grützmacher for giving me the opportunity of working and writing my thesis in PGI-9.

Distinguishable appreciation belongs to my friend and helpful supervisor Dr. Peter Schüffelgen. In the beginning of my thesis, he introduced everything in detail very patiently. Everytime when I faced with challenges, he always provided me with supportive and constructive opinions.

Appreciate dear Prof. Dr. Lars Peters for spending his precious time to instruct my master thesis.

Abdur Rehman Jalil is a very kind colleague. He has rich experience about deposition and characterization of advanced materials. He helped me how to improve the deposited materials.

Thanks to Konrad Wirtz. He taught me how to use MOVPE system. I learned much knowledge about MOVPE and the lab. When the machine was broken, he could always fix the system quickly. Without him, I can not finish my work on time.

I want to thank Dr. Gregor Mussler and Dr. Alexander Shkurmanov for delivering high quality XRD data. Alex could always test my new samples. It kept regular running of my work.

I want to thank the staff in HNF for their introduction and help. Special thanks to Dr. Elmar Neumann for maintaining the SEMs, Stephany Bunte for her work on the saw.

Thanks to Benjamin Bennemann for the introduction of AFM and maintaining AFM system.

Here, I want to also thank all of the colleagues in my group, Qi Shu, Michael, Tobias, and Max helped me a lot.